AD-A123 054 STUDIES OF THE LITHIUM ELECTRODE IN OXYCHLORIDE SOLVENTS(U) EIC LABS INC NEWTON MA G L HOLLECK ET AL. DEC 82 C-948 ARO-16116.2-CH DAAG29-78-C-0048 1/1

UNCLASSIFIED F/G 7/4 NL

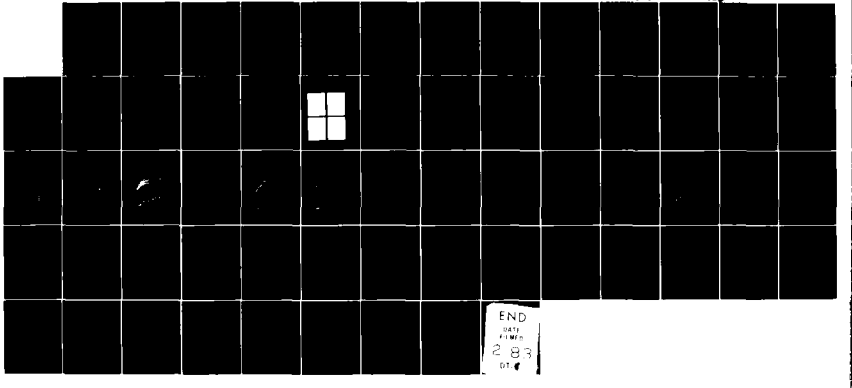

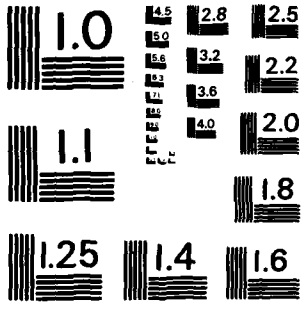

MICROCOPY RESOLUTION TEST CHART
NATIONAL BUREAU OF STANDARDS - 1963 - A

ARO 16116.2-CH

(12)

STUDIES OF THE LITHIUM ELECTRODE IN OXYCHLORIDE SOLVENTS

FINAL REPORT

Covering Period May 1, 1979 to April 30, 1982

G. L. Holleck
K. D. Brady
M. Yaniv
K. M. Abraham

December 1982

U. S. Army Research Office
P. O. Box 12211
Research Triangle Park, North Carolina 27709

Contract No. DAAG29-79-C-0045

EIC Laboratories, Inc.
67 Chapel Street
Newton, Massachusetts 02158

Approved for Public Release; Distribution Unlimited.

The view, opinions, and/or findings contained in this report are those of the author(s) and should not be construed as an official Department of the Army position, policy, or decision, unless so designated by other documentation.

UNCLASSIFIED

SECURITY CLASSIFICATION OF THIS PAGE (When Data Entered)

REPORT DOCUMENTATION PAGE	READ INSTRUCTIONS BEFORE COMPLETING FORM
1. REPORT NUMBER	2. GOVT ACCESSION NO. AD-A123054 / 3. RECIPIENT'S CATALOG NUMBER
4. TITLE (and Subtitle) STUDIES OF THE LITHIUM ELECTRODE IN OXYCHLORIDE SOLVENTS	5. TYPE OF REPORT & PERIOD COVERED FINAL REPORT 1 May 1979-30 April 1982
	6. PERFORMING ORG. REPORT NUMBER C-548
7. AUTHOR(s) G. L. Holleck, K. D. Brady, M. Yaniv and K. M. Abraham	8. CONTRACT OR GRANT NUMBER(s) DAAG29-79-C-0045
9. PERFORMING ORGANIZATION NAME AND ADDRESS EIC Laboratories, Inc. 67 Chapel Street Newton, MA 02158	10. PROGRAM ELEMENT, PROJECT, TASK AREA & WORK UNIT NUMBERS
11. CONTROLLING OFFICE NAME AND ADDRESS U.S. Army Research Office P. O. Box 12211 Research Triangle Park, NC 27709	12. REPORT DATE December 1982
	13. NUMBER OF PAGES 54
14. MONITORING AGENCY NAME & ADDRESS(if different from Controlling Office)	15. SECURITY CLASS. (of this report) Unclassified
	15a. DECLASSIFICATION/DOWNGRADING SCHEDULE

16. DISTRIBUTION STATEMENT (of this Report)

Approved for public release, distribution unlimited.

17. DISTRIBUTION STATEMENT (of the abstract entered in Block 20, if different from Report)

NA

18. SUPPLEMENTARY NOTES

The view, opinions, and/or findings contained in this report are those of the author(s) and should not be construed as an official Department of the Army position, policy, or decision, unless so designated by other documentation.

19. KEY WORDS (Continue on reverse side if necessary and identify by block number)

Lithium electrode, thionyl chloride, surface passivation, solid electrolyte films.

20. ABSTRACT (Continue on reverse side if necessary and identify by block number)

In this study we investigated the formation of protective surface films on in situ freshly exposed Li in $LiAlCl_4/SOCl_2$ electrolytes using electrochemical techniques. Based on the results we propose a film model consisting of three regions. Region I forms rapidly (less than one hour) upon exposure of a fresh surface. It has a thickness between 200 and 400 A and an apparent resistivity of $\sim 2.10^7$ Ωcm. It appears to have significant imperfection and some microporosity along the grain boundaries. This is followed by a Region

DD FORM 1 JAN 73 1473 EDITION OF 1 NOV 65 IS OBSOLETE

UNCLASSIFIED

SECURITY CLASSIFICATION OF THIS PAGE (When Data Entered)

II film which is more ordered and more compact. Its resistivity is $\sim 2.10^8$ Ωcm and it grows to 200 to 600 Å within a 20 hour period. Further growth is slow. The Region III film is porous and coarsely crystalline formed by dissolution and recrystallization of the Region II film. The Region III film does not contribute to the micropolarization measurements near the open circuit potential. The film growth kinetics can be described as a combination of a parabolic growth and a constant rate dissolution reaction.

TABLE OF CONTENTS

Section		Page
I	INTRODUCTION.	1
II	EXPERIMENTAL.	2
	1. Materials and Hardware.	2
	1.1 Experimental Cells	2
	1.2 Electrolytes	5
	1.3 Instrumentation.	6
	1.4 Measurement Procedure and Treatment of Raw Data.	6
	1.4.1 Experimental Procedure.	6
	1.4.2 Raw Data Treatment.	12
	1.5 Error and Reliability of Measurements.	12
III	RESULTS	16
	1. General Structure of the Surface Film on C.	16
	2. Variation of Electrolyte.	16
	3. Analysis of Voltage Transients.	34
	4. Film Growth Kinetics.	34
	5. Film Resistivity.	37
IV	DUSCUSSION AND CONCLUSIONS.	49
	1. Structure of the Surface Film	49
	2. Film Growth Kinetics.	51
V	REFERENCES.	54

LIST OF ILLUSTRATIONS

Figure		Page
1	"Fresh surface" cell design.	3
2	Stainless-steel compression assembly	4
3	Cell cap design and cell cap set up for experimentation.	4
4	Instrumentation configurations for a) transient response measurements, and b) steady-state measurements	7
5	Excerpts from Notebook No. 369	9
6	Transient response of film at .03 h, .63 h, 3.05 hr, and 5.97 hr.	10
7	Calculation of capacitance, resistance, and rise-time constant.	11
8	Early measurements on Li foil electrodes and fresh Li surfaces in electrolyte without specific pretreatment	17
9	Inverse capacity and resistance of films grown on fresh Li in 1.8M $LiAlCl_4/SOCl_2$	18
10	Inverse capacity and resistance values of films grown on fresh Li surfaces in 1.8M $LiAlCl_4/SOCl_2$ electrolyte pretreated with metallic Li.	19
11	Inverse capacity and resistance values of films grown on fresh Li surfaces in 1.8M $LiAlCl_4/SOCl_2$ electrolyte.	20
12	Inverse capacity and resistance of films grown on fresh Li surfaces in 1.8M $LiAlCl_4/SOCl_2$.	21
13	Inverse capacity and resistance of films grown on fresh Li surfaces in 0.5M $LiAlCl_4/SOCl_2$.	22
14	Inverse capacity and resistance values of films grown on fresh Li surfaces in $LiAlCl_4/SOCl_2$ of varying concentrations	23

LIST OF ILLUSTRATIONS
(continued)

Figure		Page
15	Inverse capacity and resistance values of films grown on fresh Li surfaces in $LiAlCl_4/SOCl_2$ electrolytes of varying concentrations	24
16	Resistance and capacity measured in experiment 8-10A upon substitution of the electrolyte	26
17	Resistance and capacity measured in experiment 9-30B upon substitution of the electrolyte	27
18	Inverse capacity vs. inverse concentration	30
19	Simplified equivalent circuit representing film capacitance and resistance	31
20	$(1/R_{exp})$ vs. electrolyte conductivity.	32
21	Normalized voltage-time transient.	35
22	(1/C) vs. t and R vs. t plots illustrating erratic, parallel changes in R and (1/C).	38
23	Inverse square capacitance vs. time plots (parabolic plots)	39
24	$\partial(1/C)/dt$ vs. capacitance	40
25	$\partial(1/C)/dt$ vs. capacitance	41
26	Inverse capacity vs. resistance.	44
27	Inverse capacity vs. resistance.	45
28	Inverse capacity vs. resistance for three cuts of experiment 7-05A.	46
29	Schematic illustration of the proposed three region model of the film formed on fresh Li surface upon exposure to $LiAlCl_4/SOCl_2$ electrolytes	50

LIST OF TABLES

Table		Page
1	MEASUREMENT ERROR EVALUATION.	15
2	SUMMARY OF MEASURED INVERSE CAPACITY AND RESISTANCE VALUES OF FILMS GROWN ON FRESH Li SURFACES AFTER EXPOSURE FOR 20 HOURS TO VARIOUS $LiAlCl_4/SOCl_2$ ELECTROLYTES.	25
3	CHANGES IN CAPACITANCE AND RESISTANCE OF PREGROWN FILMS IMMERSED IN ELECTROLYTES OF DIFFERENT CONCENTRATIONS.	28
4	ESTIMATE OF MINIMUM Li FILM POROSITY FROM THE DEPENDENCE OF THE OBSERVED FILM RESISTANCE ON ELECTROLYTE CONCENTRATION	33
5	VOLTAGE TIME TRANSIENT PARAMETERS	36
6	RATE CONSTANTS FOR FILM GROWTH AND FILM DISSOLUTION	42
7	SPECIFIC RESISTIVITIES OF FILMS GROWN ON FRESH Li SURFACES.	47
8	SPECIFIC RESISTIVITIES OF FILMS GROWN ON FRESH Li SURFACES.	48

I. INTRODUCTION

When this study was initiated it was already generally accepted that the Li electrode in thionyl chloride ($SOCl_2$) was covered by a surface film which protects it from direct rapid reaction with the strongly oxidizing solvent while still allowing electrochemical oxidation of the Li. Earlier studies of such films which consist essentially of LiCl were carried out and reviewed by Dey (1,2). These films appeared relatively thick and coarse crystalline suggesting that they do not exhibit the actual barrier properties leading to the protection of the Li surface from further corrosive attack. We suspected that this function was assumed by a thin compact underlying film. It was the objective of this study to characterize the electrochemical properties of this film during the early stages of formation. Furthermore we wanted to avoid the uncertainty resulting from the ever present preexisting surface films on Li by creating a fresh Li surface <u>in situ</u> within the electrolyte solution.

During the course of this study several reports dealing with the films on Li electrodes were published (3,9). In the discussion section we will compare these results with our findings.

II. EXPERIMENTAL

1. Materials and Hardware

Because of the reactive nature of both lithium and thionyl chloride, all experiments were conducted in a Vacuum Atmospheres glove box filled with argon (<10 ppm O_2; <5 ppm H_2O) and equipped with a dri-train which maintained the H_2O level below the limit of detection using $TiCl_4$, except during periods of dri-train regeneration.

1.1 Experimental Cells

Experimental cells for measurement and fresh surfaces were constructed from Macor glass, a Corning machinable ceramic which is non-porous and resistant to the experimental environment. The design of one of these cells is given in Figure 1. Viewed from above, the cell consists of a rectangular chamber 3.5 cm deep having a hole on one side. During experimentation this chamber is filled with electrolyte, and lithium is extruded from the hole and then cut to expose a clean surface. The last 10 mm of the lithium channel has a conical taper from a diameter of 12.5 mm to 10.0 mm. This taper compresses the lithium and prevents backflow of electrolyte into the channel.

The mechanical ruggedness of the cell is enhanced by the stainless steel compression assembly shown in Figure 2. Lithium extrusion is achieved by fitting a screw-piston onto this jig.

The cell cap is diagrammed in Figure 3a, b. It is made of either Macor or Teflon, and its small end fits loosely into the cell chamber. The perspective sketch (Fig. 3b) illustrates the cap appearance immediately before experimentation, with wiring and lithium electrodes attached. The reference electrode is smaller than the auxiliary, it is generally cut to a point, and when the cap is placed onto the cell, it is positioned between the working (extruded and cut) electrode and the auxiliary electrode.

For later experiments, a Viton O-ring and a compression clamp were fit onto the cap so as to provide a better seal. The second Macor cell differs from the first cell having a 2.5 cm diameter hole at the top of the chamber. Fitting a close-tolerance round Teflon cap into the circular cell-top provides an excellent seal without using the clamp and O-ring.

The nickel wires leading from the reference and auxiliary electrodes are connected directly to BNC coaxial-cable connectors which provide direct attachment to the electronic instrumentation. The working electrode is

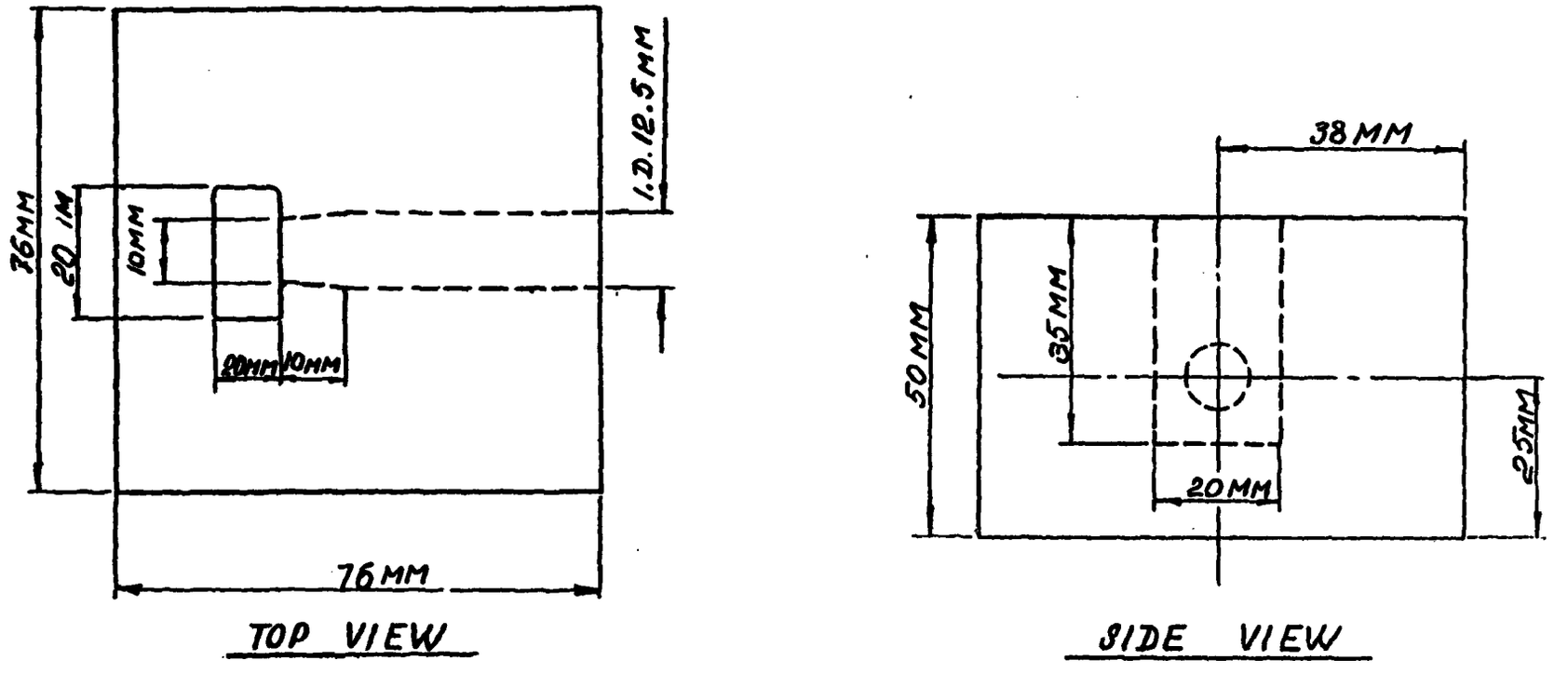

Fig. 1. "Fresh-surface" cell design.

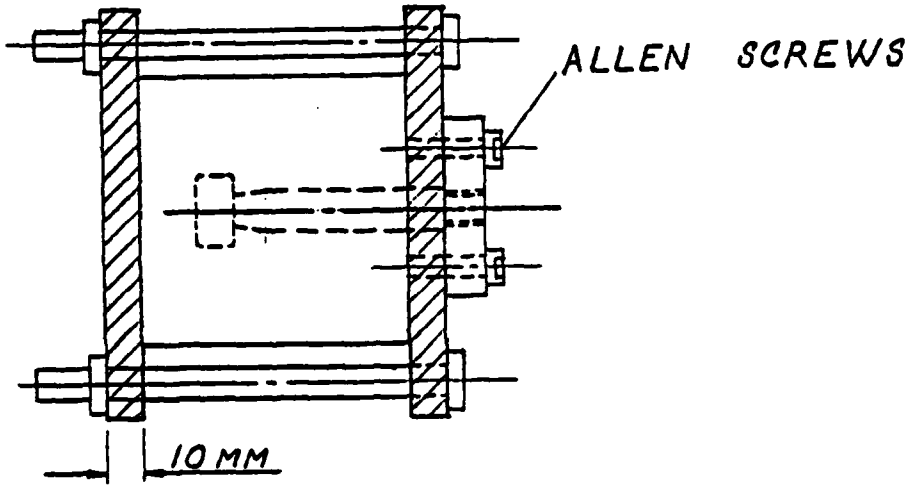

Fig. 2. Stainless-steel compression assembly.

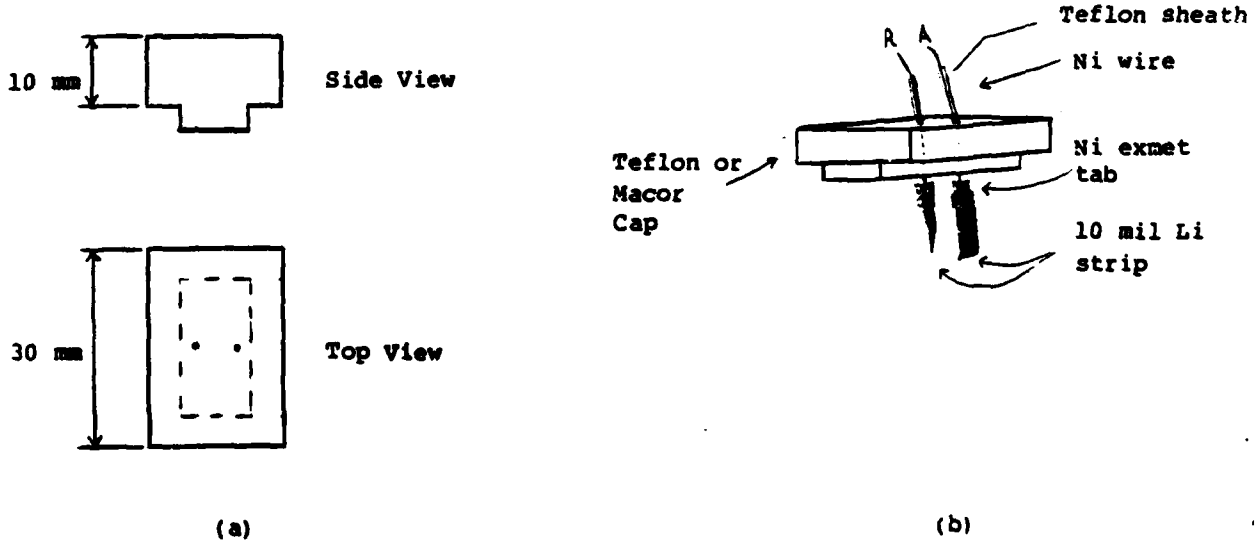

Fig. 3. a) Cell cap design.
b) Cell cap set up for experimentation.

connected via an alligator clip which attaches to the stainless steel compression assembly.

Measurements on Li foil electrodes were conducted in glass cells. These were constructed from O-ring joints (ID 50 mm). Electrodes were prepared from two sheets of 10 mil lithium foil (99.9% Foote Mineral Co.) pressed on both sides of Ni screen. The sandwich structure of the electrodes ensures that nickel was not exposed to the solution where it might have created a local cell with the lithium. The counter electrode was a cylinder 3 cm in diameter and 3 cm in height. Two parallel 1 cm^2 ribbons placed in the center served as working and reference electrodes. The Ni screen stripped at the upper part of the electrodes was spot welded to the tungsten rods sealed to the cell cap.

1.2 Electrolytes

The solvent used in preparing electrolytes was Eastman Kodak thionyl chloride (No. 246). Analysis of this as-received product by infrared absorption spectroscopy indicated the presence of trace quantities of sulfuryl chloride (SO_2Cl_2) and sulfur chlorides. Various attempts in solvent purification including double-distilling from a mixture with triphenyl phosphite (1) [$(PhO)_3P$] and lithium chips, did not result in improved solvent quality.

Prior to electrolyte preparation, salts were vacuum-dried to remove traces of water. Anhydrous aluminum trichloride (Fluka puriss, iron free) was heated to 90°C at a pressure of ~100 μm Hg for 16 hours. Lithium chloride (Fisher Certified) was heated to 150°C under a pressure of ~50 μm Hg for 16 hours.

$LiAlCl_4/SOCl_2$ electrolytes were prepared by two methods. During the earlier experiments we used the method of successive dissolution. In this method, $AlCl_3$ is first dissolved in the solvent, then LiCl is added. Lithium chloride is normally insoluble in $SOCl_2$, but in the presence of $AlCl_3$ it slowly dissolves due to the Lewis-acid/Lewis-base neutralization:

$$LiCl + AlCl_3 \xrightarrow{SOCl_2} Li^+ + AlCl_4^-$$

In the second method used for later experiments, lithium tetrachloroaluminate ($LiAlCl_4$) is prepared in a melt, purified by electrolysis between Al electrodes for at least 48 hours and then added to the solvent. In both cases, excess LiCl (~10%) is added to suppress free $AlCl_3$.

Once mixed, electrolyte appearance varies from colorless to slightly brown-tinged. Electrolytes which were treated with lithium are yellowish. Electrolytes prepared by double dissolution were filtered after only ~2 hours of equilibration. This may have resulted in slightly acidic (i.e.,

excess $AlCl_3$) solutions (2). In most electrolytes prepared from the electrolyzed salt, the excess LiCl was never filtered out. A description of each electrolyte used in experimentation, including its method of preparation, age, and period of equilibration with LiCl is given in Section III (Table 2).

1.3 Instrumentation

For fast galvanostatic pulses we used a Wavetek Model 185 Sweep Generator. In the square-wave mode, it demonstrates a rise-time of 0.3 μs. For constant current applications we used an EG&G/PAR Model 173 Potentiostat/Galvanostat equipped with a Model 176 Current Follower. While this instrument displays excellent output accuracy, with the moderate loads encountered in our work (10 Ω-10 kΩ) it typically demonstrated a rise time of ~20 μs. It was therefore used only in steady-state (8 ms pulse) resistance measurements. Our measurement system consisted of a Tektronix 5103N Oscilloscope with a 5B10N Time Base/Amplifier and a 5A20N Differential Amplifier. Signals were recorded using a Tektronix Model C-5 Oscilloscope Camera.

The instrument/cell configurations for transient-response and steady-state measurements are shown in Figure 4a,b. Switch A allows easy interchange of the two configurations. In a few experiments designed to examine the RC-type approach to steady state, the configurations is the same as for steady-state except the time scale is magnified by 10X (100 μs/div horizontal). Most electrical connections are made with RG 58c/u coaxial cable and BNC type connectors. Not pictured in Figure 4 is a set of switches enabling the experimentor to access either of the two cells.

1.4 Measurement Procedure and Treatment of Raw Data

The predominant techniques applied in our investigation consisted of monitoring the voltage response of the filmed electrode upon application of a galvanostatic pulse. Such measurements were carried out as a function of time from exposure of a fresh Li surface to the oxychloride electrolyte and were used to determine the capacity and resistance of the surface films. The experimental procedures are described in more detail below.

1.4.1 Experimental Procedure

The electrochemical cell was set up at least one day prior to the test run to allow the cell and the reference and counter electrodes to equilibrate with the electrolyte to be used. Test measurements were conducted to check for clean electrical contacts and proper operation of the setup. On the day of the measurement, the Li working electrode is extruded ~0.5 mm, the electrolyte is removed using a pipette, the cell and electrodes are rinsed with fresh electrolyte of the same type and then the cell is filled with fresh electrolyte. This is followed by in situ cutting of

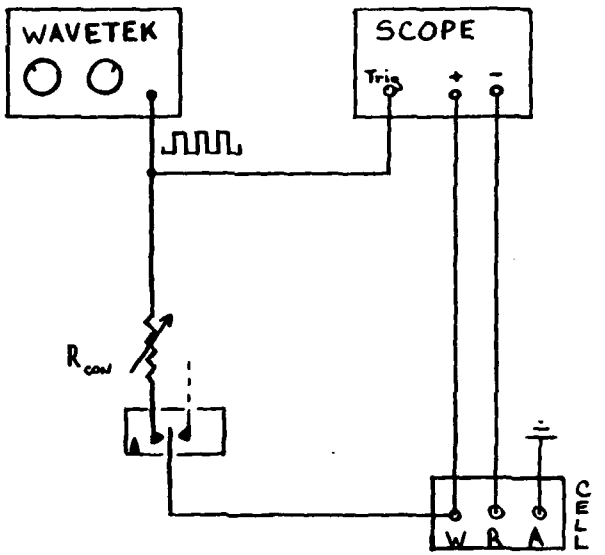

Wavetek output: 100 KHz
Bipolar square wave
20 V ptp
continuous mode

Controlling Resistor: 100-300 KΩ

Scope Setting: 1 µs/div horizontal
2 mV/div vertical
Differential mode (W - R)

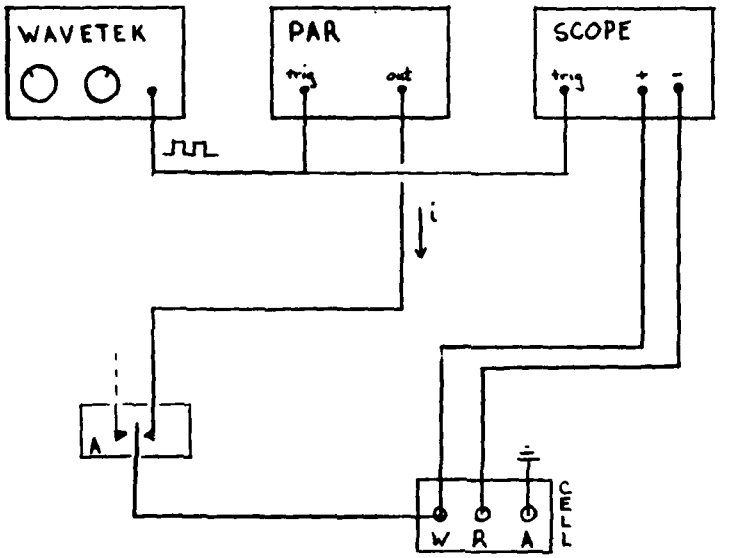

Generator Output: 1000 Hz
monopolar square wave
10 V
manual trigger mode

PAR Setting: Control I
Trigger (track)
1-500 µA

Scope Setting: 1 ms/div horizontal
2 mV/div vertical
Differential mode

Fig. 4. Instrumentation configurations for a) transient response measurements, and b) steady-state response measurements.

the working electrode with a sharp ceramic knife. The cut-off Li is removed (it generally adheres to the knife) and the cell cover is replaced. The time of electrode cutting marks the start of this experiment.

Both capacitance ("transient response") and resistance ("steady-state response") measurements are made 5 or 6 times within the first hour since this is a period of rapid change, particularly for the capacitance. An example of an actual notebook record is shown in Figure 5. The following data are recorded for each measurement: picture number, type of measurement (C, R, or R'), vertical 'scope deflection, horizontal 'scope deflection, control resistance or current-pulse magnitudes, and time of day. Six measurements were made in the first hour, followed by one measurement per hour for the remainder of the day.

The evolution of the transient measurements is shown in Figure 6. Immediately after cutting, the response resembles a square wave. After 7 hours, however, voltage across the film increases much more rapidly and the response resembles a triangle wave. This is interpreted as a decreasing capacitance across the film as the film grows thicker. Figure 7a illustrates the method of calculating capacitance from these photographs.

The evolving steady-state response is not so readily displayed since successively lower measuring currents are used as the film becomes more resistive. Figure 7b shows a typical measurement and the method of calculating the film resistance. To examine the approach to steady-state, the initial portion ($t<0.8$ ms) of this series of traces is magnified 10X. The method of calculation of the time constant τ is illustrated in Figure 7c. The capacitance, resistance, and time constant are calculated and plotted against growth time. Most films were monitored over the first 24 hours of growth. In some cases film growth was followed over several days.

Some films were grown in one electrolyte and then examined in different electrolytes. This involves careful exchange of the electrolyte without harming the Li surface film. The absence of irreversible changes was established by returning to the original electrolyte after such a measuring series. Typically, potential-time measurements were conducted immediately following an electrolyte change and then after 30 and 90 minutes.

Other measurements included evaluation of the high field response (Tafel behavior) and of film rupture during prolonged high current pulses. The high field response was measured by a procedure similar to that of resistance measurements, except that a higher applied current ($\sim$20 mA/cm^2) induces a voltage response (typically $\sim$0.5V) which increases as the logarithm of current. By plotting log i vs. V, the Tafel slope b was determined.

The behavior of a few filmed electrodes was studied by passing high film rupturing galvanostatic currents of 10 mA/cm^2. The electrode potential was recorded from the oscilloscope for the initial transient and on a stripchart recorder for polarizations up to 10 minutes duration.

Photo	Var.	'Scope Deflection, R_{con}, I_{AP}			Time
1A	C	2 mV	1 μs	134 kΩ	9:58
2A	R	2 mV	1 ms	500, 400, 300, 200, 100 μA	9:59
3A	C	2 mV	1 μs	134 kΩ	10:03
4A	R	2 mV	1 ms	500, 400, 300, 200, 100 μA	10:04
5A	C	2 mV	1 μs	134 kΩ	10:08
6A	R	2 mV	1 ms	500, 400, 300, 200, 100 μA	10:09
7A	C	2 mV	1 μs	134 kΩ	10:15
8A	A	2 mV	1 ms	400, 320, 240, 160, 80 μA	10:16
23A	C	2 mV	1 μs	134 kΩ	5:15
24A	R	2 mV	1 ms	8, 6.4, 4.8, 3.2, 1.6 μA	5:17
24A'	R'	2 mV	100 μs	8, 6.4, 4.8, 3.2, 1.6 μA	5:18
25A	C	2 mV	1 μs	234 kΩ	9:12
26A	R	2 mV	1 ms	4, 3.2, 2.4, 1.6, 0.8 μA	9:13
26A'	R'	2 mV	100 μs	4, 3.2, 2.4, 1.6, 0.8 μA	9:14
Electrolyte change: 1.0 → 1.8M $LiAlCl_4/SOCl_2$ at 10:28					
29A	C	2 mV	1 μs	234 kΩ	10:31
30A	R	2 mV	1 ms	4, 3.2, 2.4, 1.6, 0.3 μA	10:32
30A'	R'	2 mV	100 μs	4, 3.2, 2.4, 1.6, 0.3 μA	10:33
31A	C	2 mV	1 μs	234 kΩ	11:01
32A	R	2 mV	1 ms	4.5, 3.6, 2.7, 1.8, 0.9 μA	11:03
32A'	R'	2 mV	100 μs		11:04
Electrolyte change: 0.5M → 1.0M at 3:42					
47A	C	2 mV	1 μs	234 kΩ	3:44
48A	R	2 mV	1 ms	4, 3.2, 2.4, 1.6, 0.8 μA	3:45
48A'	R'	2 mV	100 μs	4, 3.2, 2.4, 1.6, 0.8 μA	3:46
49A	C	2 mV	1 μs	234 kΩ	4:11
50A	R	2 mV	1 ms	4.5, 3.6, 2.7, 1.8, 0.9 μA	4:12
50A'	R'	2 mV	100 μs	4.5, 3.6, 2.7, 1.8, 0.9 μA	4:13
51A	C	2 mV	1 μs	234 kΩ	5:15
52A	R	2 mV	1 ms	4, 3.2, 2.4, 1.6, 0.8 μA	5:16

Fig. 5. Excerpts from Notebook No. 369, pp. 121-122. Experiment 8-10A.

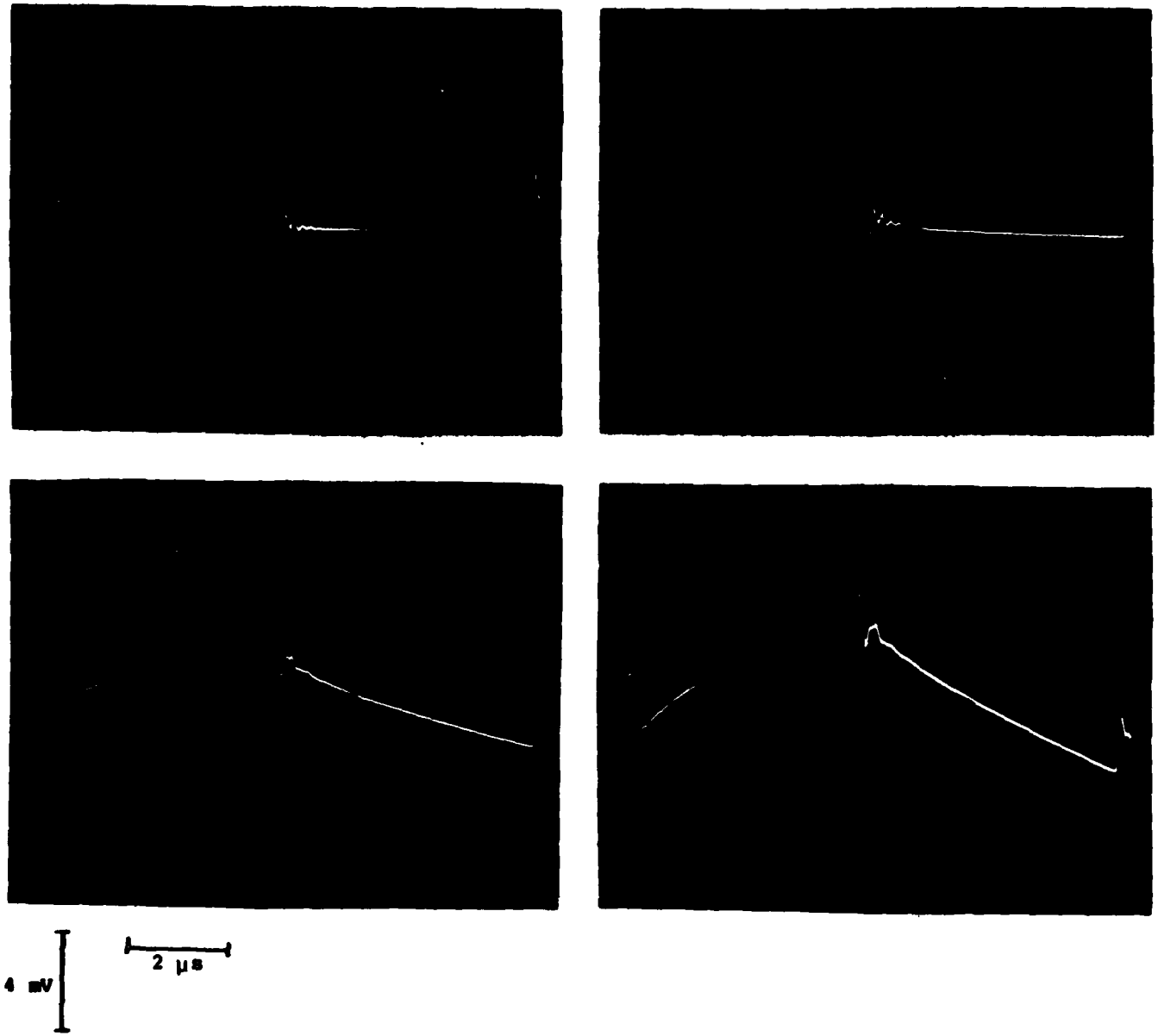

Fig. 6. Transient response of film at .03 h, .63 h, 3.05 h, and 5.97 h. Experiment 8-10A.

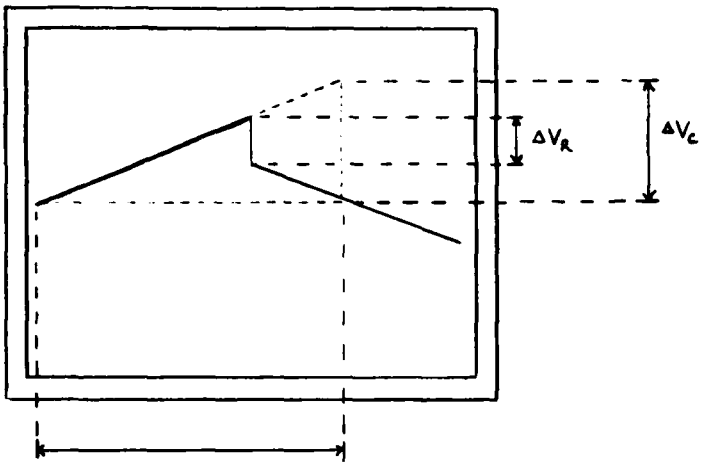

Δt (50 mm) = 5.88 μs

Solution Resistance

$R_{sol} = R_{con}\ (\Delta V_R/20V)$

Film Capacitance

$$C = \left(\frac{20V}{R_{con}}\right)\Big/\left(\frac{\Delta V_C}{\Delta t}\right) \qquad (a)$$

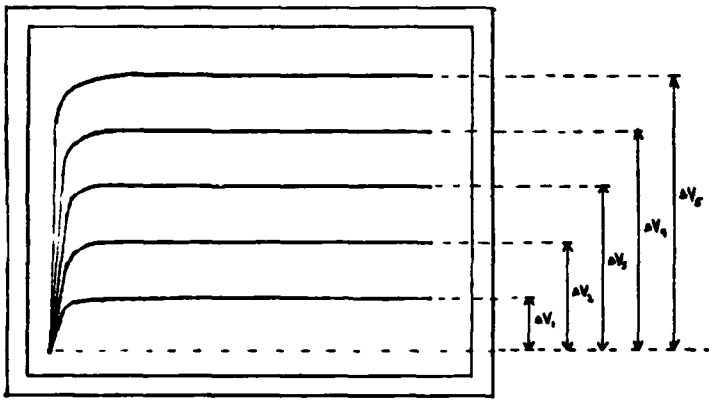

Pulse duration: 8 ms

Film Resistance

$$R_f = \frac{d(\Delta V)}{di}$$

Slope of ΔV_n vs. i_n is calculated by linear regression.

(b)

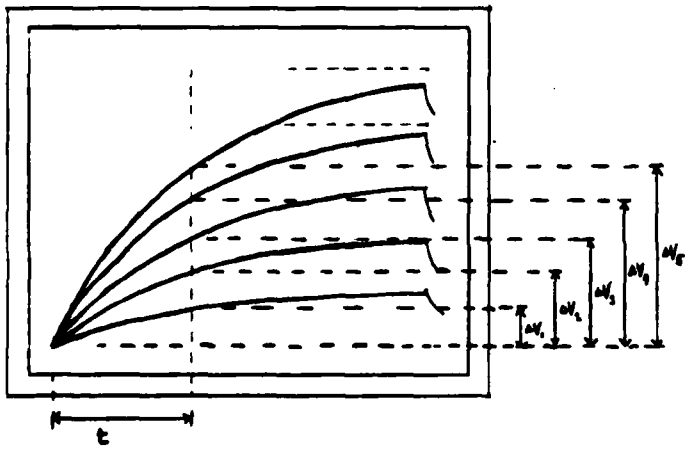

Pulse duration: 0.8 ms

Rise-Time Constant τ

Apparent resistance is calculated for t = 100, 300, 500, and 800 μs. τ is evaluated from logarithmic curve fit:

$$-\log\left[1-\frac{R(t)}{R_f}\right] = \left(\frac{1}{\tau}\right)t. \qquad (c)$$

Fig. 7. Calculation of capacitance, resistance, and rise-time constant.

1.4.2 Raw Data Treatment

The experimental cell has been diagrammed below, together with a schematic representing the electronic behavior of the system.

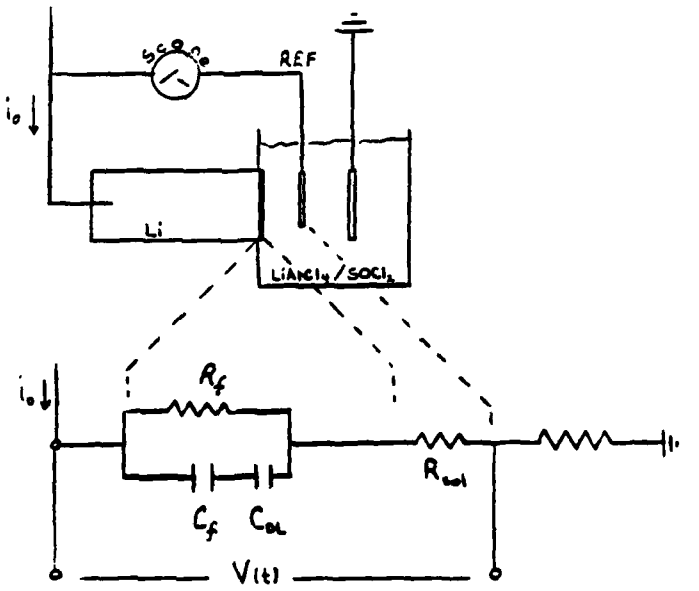

From this schematic, the voltage between the working and reference electrodes is:

$$V(t) = i_o[R_{sol} + (R_f\ 1\text{-}\exp(-t/R_fC))];\ \tau = R_f\bar{C}$$

and

$$\left(\frac{dV(t)}{dt}\right)_{t\to o} = i_o/\bar{C} \quad \text{where} \quad \bar{C} = \frac{C_fC_{DL}}{C_f+C_{DL}}$$

In most cases, the double layer capacitance C_{DL} is much greater than the film capacitance, and $C \cong C_f$. These are the formula upon which the calculations of Figure 7 are based.

1.5 Error and Reliability of Measurements

During our study of thin films we also examined the reactance of our measurement system. This was indicated, given the relatively high fre-

quencies employed and the length of cabling required to bring the signals in and out of the argon glove box.

We proceeded by inserting parallel RC-circuits of known resistance and capacitance into various points of the measurement circuitry. Points of insertion are 1) between the waveform generator and the controlling resistor; 2) between the controlling resistor and the cell; and 3) between the cell and ground. By comparing the voltage response of the calibrated circuits we were able to analyze the system reactance.

For each of these series of measurements, it has been possible to explain the circuit reactance by inserting an RC "leg" on either side of the calibrated circuit, which leg represents the cabling and instrumentation impedance to ground. This concept is now extended to real cell measurements.

In the diagram below, the cell is enclosed in dashed lines and has a resistance R_C and capacitance C_C. V_C is the voltage between working and reference electrodes as measured on the oscilloscope. The two RC legs have an unknown capacitance and a resistance of 1M Ω.

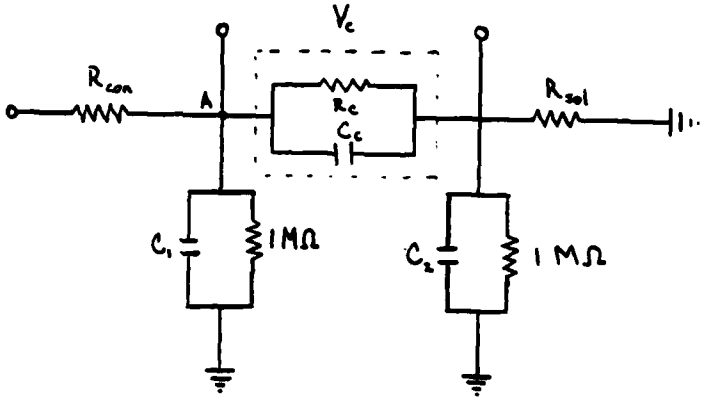

Based on our observations, the following statements are justified.

1) The current entering node A from the control resistor is essentially constant over the duration of the 5 μs pulse.

2) C_1 and C_2 are no greater than 8000 pF.

To examine the error in measuring C_c, we start by considering the ideal behavior of the cell voltage:

$$V_c = \frac{V_o}{R_{con}} R_c[1-e^{-t/R_cC_c}]$$

The voltage at node A relative to ground is

$$V_A \cong V_c + \frac{V_o}{R_1} R_{sol}$$

and

$$\frac{DV_A}{dt} = \frac{V_o}{R_{con}C_c} e^{-t/R_cC_c}$$

The current flowing through the impedance leg at node A is

$$i_A = C_1 \frac{dV_A}{dt} = \left(\frac{C_1}{C_c}\right) \frac{V_o}{R_{con}} e^{-t/R_cC_c}$$

Current through the cell is then

$$i_c = \frac{V_o}{R_{con}} \left[1-\left(\frac{C_1}{C_c}\right) e^{-t/R_cC_c}\right]$$

This represents a first-order approximation of the actual current flowing through the cell. It is smaller than the theoretical current by a factor $[1-(\frac{C_1}{C_c})\ e^{-t/R_cC_c}]$. The maximum error that results is listed below for the encountered range of cell capacitances.

In the case of old films under dilute electrolytes, the error cannot be neglected. Since C_1 is in parallel with C_c, the error is positive and the apparent capacitance will be greater than the real cell capacitance.

To examine this effect, dummy cells were constructed and inserted into the circuit in place of the fresh-surface cell. The dummy cell capacitances and the measured capacitances are compared in Table 1. These values illustrate the error due both to the measuring circuit reactance and to the limited precision with which measurements may be taken from photographs of the oscilloscope trace. Since $\left(\frac{\Delta V}{\Delta t}\right)$ is smallest for a large capacitance, measurement error is largest under conditions where the reactance error is smallest.

TABLE 1

MEASUREMENT ERROR EVALUATION

Errors Due to System Reactance

Typical Growth Stage	C_c (μF)	C_l (pF)	Maximum Error (%)	Error @ 4 μs[1]
Initial	0.500	4000	0.8	0.8
		8000	1.6	1.6
Late	0.100	4000	4.0	3.9
		8000	8.0	7.9
Late (dilute electrolyte)	0.060	4000	6.7	6.5
		8000	13.3	13.0

[1]Assuming typical cell resistance of 3000 Ω.

Comparison of Actual and Measured Capacitances

Dummy Cell	Capacitance (μF) Actual	Measured
1	0.100	0.110
2	0.010	0.0163
3	0.001	0.0051
4	0	847 pF

III. RESULTS

During this investigation we generated a large body of data consisting especially of capacity and resistance measurements on surface films covering freshly exposed Li in various electrolytes as a function of time. In the following we summarize representative results.

Earlier measurements on Li foil electrodes and fresh Li surfaces in electrolyte without specific pretreatment are summarized in Figure 8. The electrolytes were prepared by successive dissolution of the salts. Films on Li foil electrodes were found to grow much more rapidly during the early stage than films on a freshly in situ exposed Li surface. After several days film capacity reaches a plateau with little further change. The time dependence of the film resistance from micropolarization measurements parallels that of the inverse film capacitance.

The bulk of our measurements were carried out on in situ generated fresh Li surfaces concentrating on the initial film growth period in the range of 1 to 3 days. Figures 9 to 15 show characteristic values of inverse capacity, 1/C (μF^{-1} cm^2), and film resistance, R (Ω cm^2), as a function of time for films grown in various electrolytes. The electrolyte composition and history is summarized in Table 2. For easier comparison we tabulated the capacity and resistance values after 20 hours and included them also in Table 2.

1. General Structure of the Surface Film on C

Experiments were carried out with the objective to elucidate two issues: (1) Is the surface film growing on fresh Li surfaces compact or porous and (2) to what degree do the measured values of capacitance and resistance reflect film properties?

2. Variation of Electrolyte

A number of films pre-grown in different electrolytes, at different $LiAlCl_4$ concentrations and for different times between 24 and 73 hours were exposed to electrolytes of various concentrations. Capacitance and resistance of each film were monitored as a function of electrolyte concentration and time. Characteristic runs are shown in Figures 16 and 17. Additional data is summarized in Table 3. Figures 16 and 17 are typical in showing the difference in the rate of stabilization of the C and R values following a change in solution concentration (it is quite rapid in the film 8-10A, Figure 16, and more sluggish in experiment 9-30A, in particular when changing from very high to very low electrolyte concentrations) and in

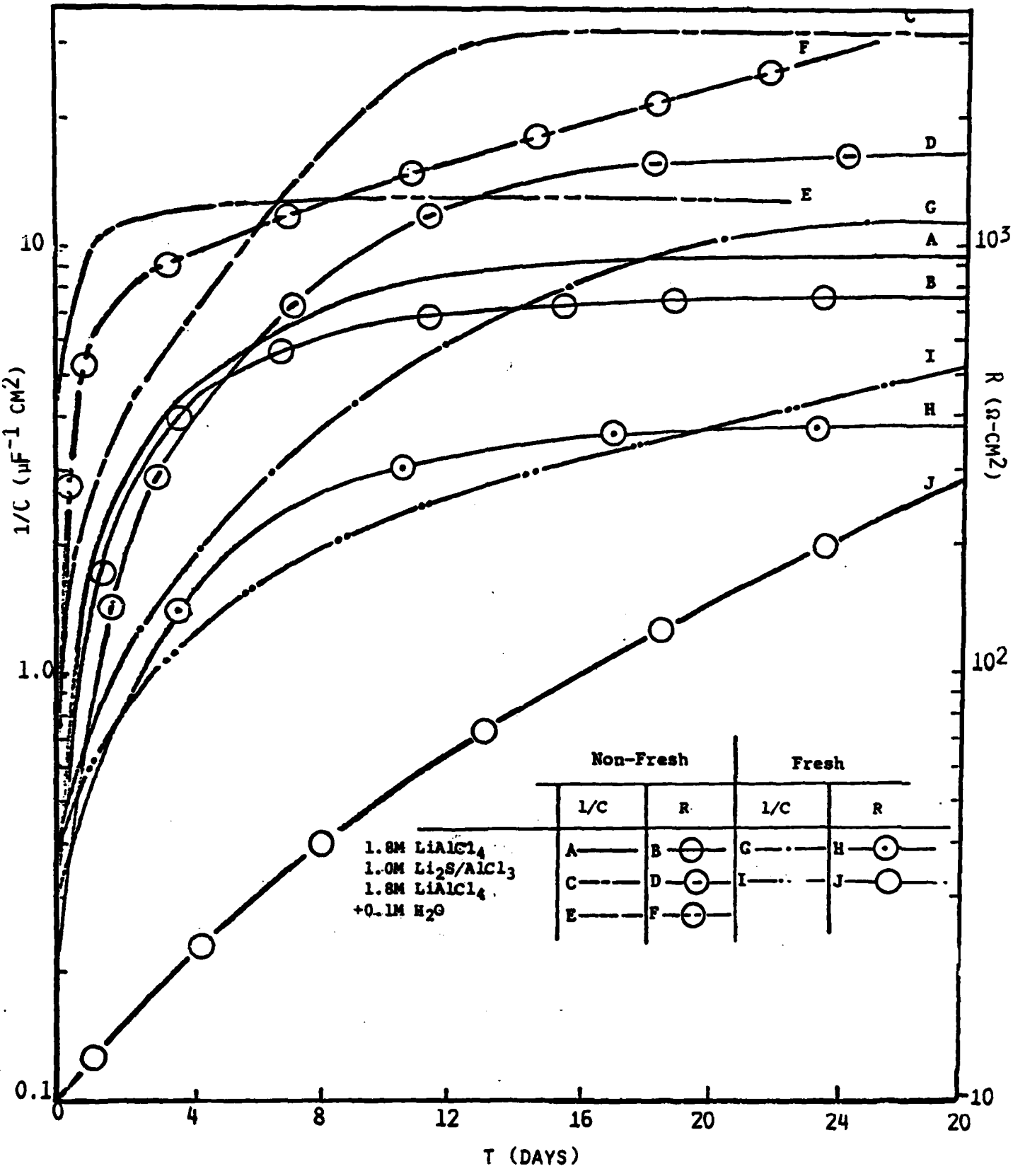

Fig. 8. Early measurements on Li foil electrodes and fresh Li surfaces in electrolyte without specific pretreatment.

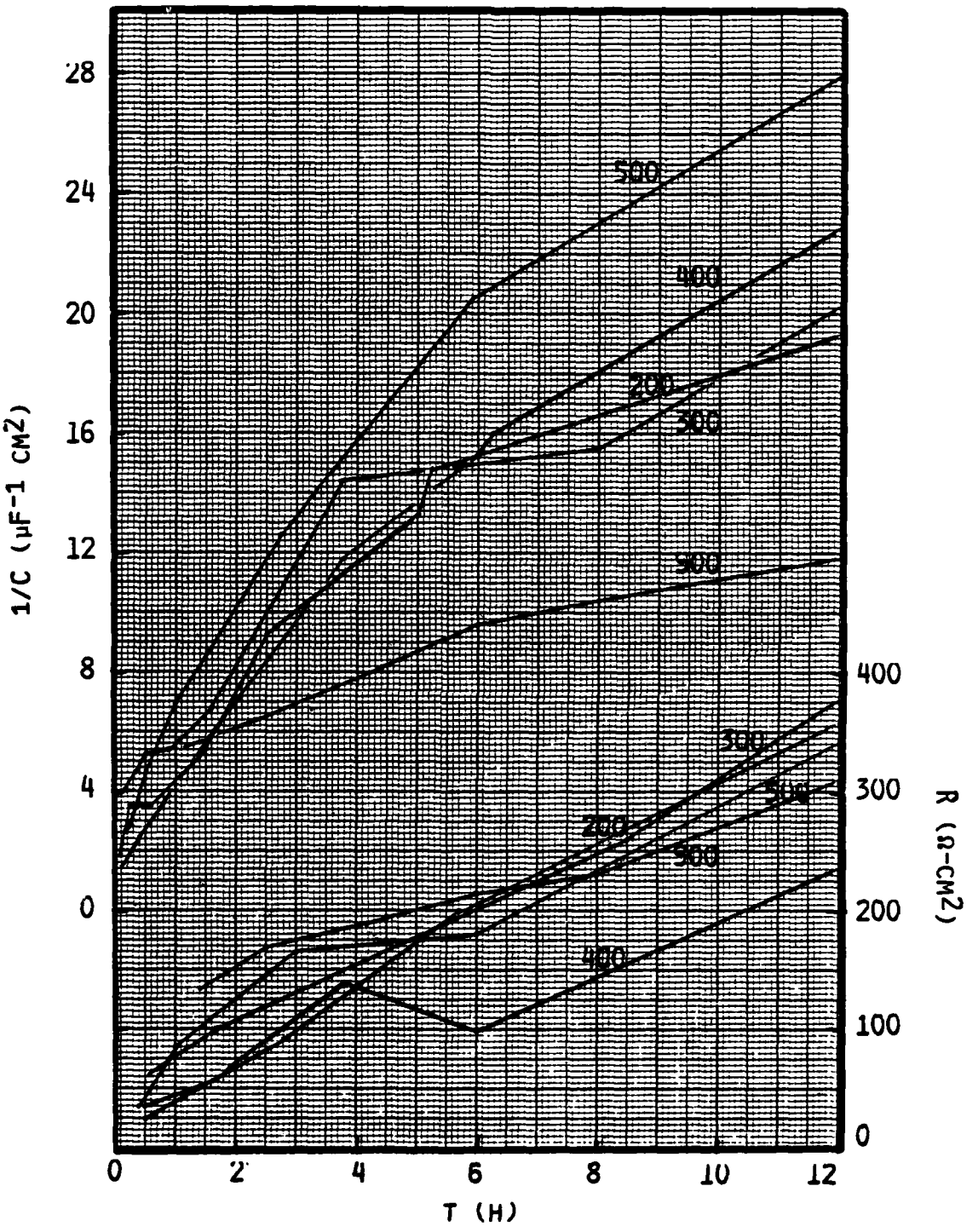

Fig. 9. Inverse capacity and resistance of films grown on fresh Li in 1.8M $LiAlCl_4/SOCl_2$. Series 1-xxx.

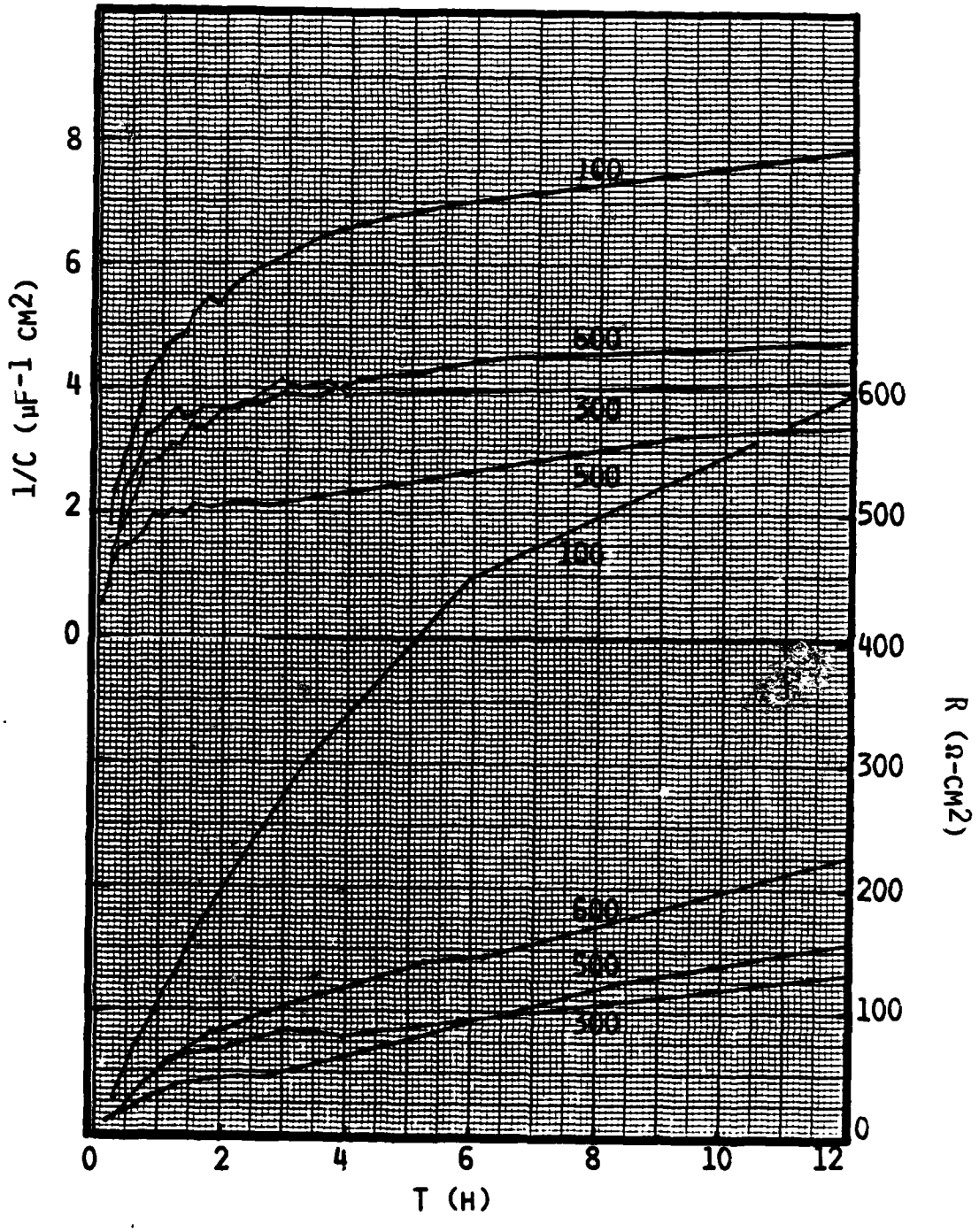

Fig. 10. Inverse capacity and resistance values of films grown on fresh Li surfaces in 1.8M $LiAlCl_4/SOCl_2$ electrolyte pretreated with metallic Li. Series 5-xxx.

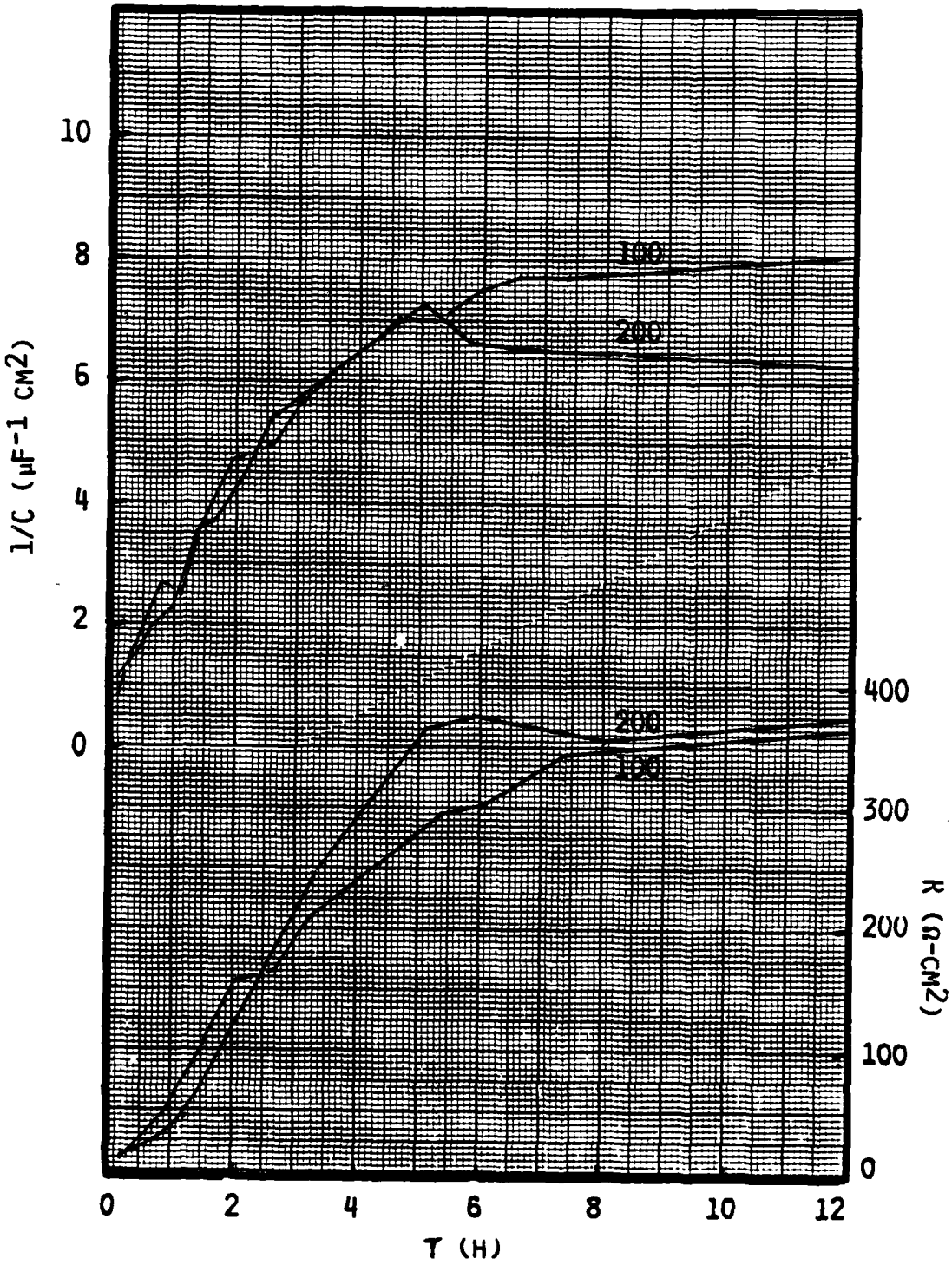

Fig. 11. Inverse capacity and resistance values of films grown on fresh Li surfaces in 1.8M $LiAlCl_4/SOCl_2$ electrolyte. Series 6-xxx.

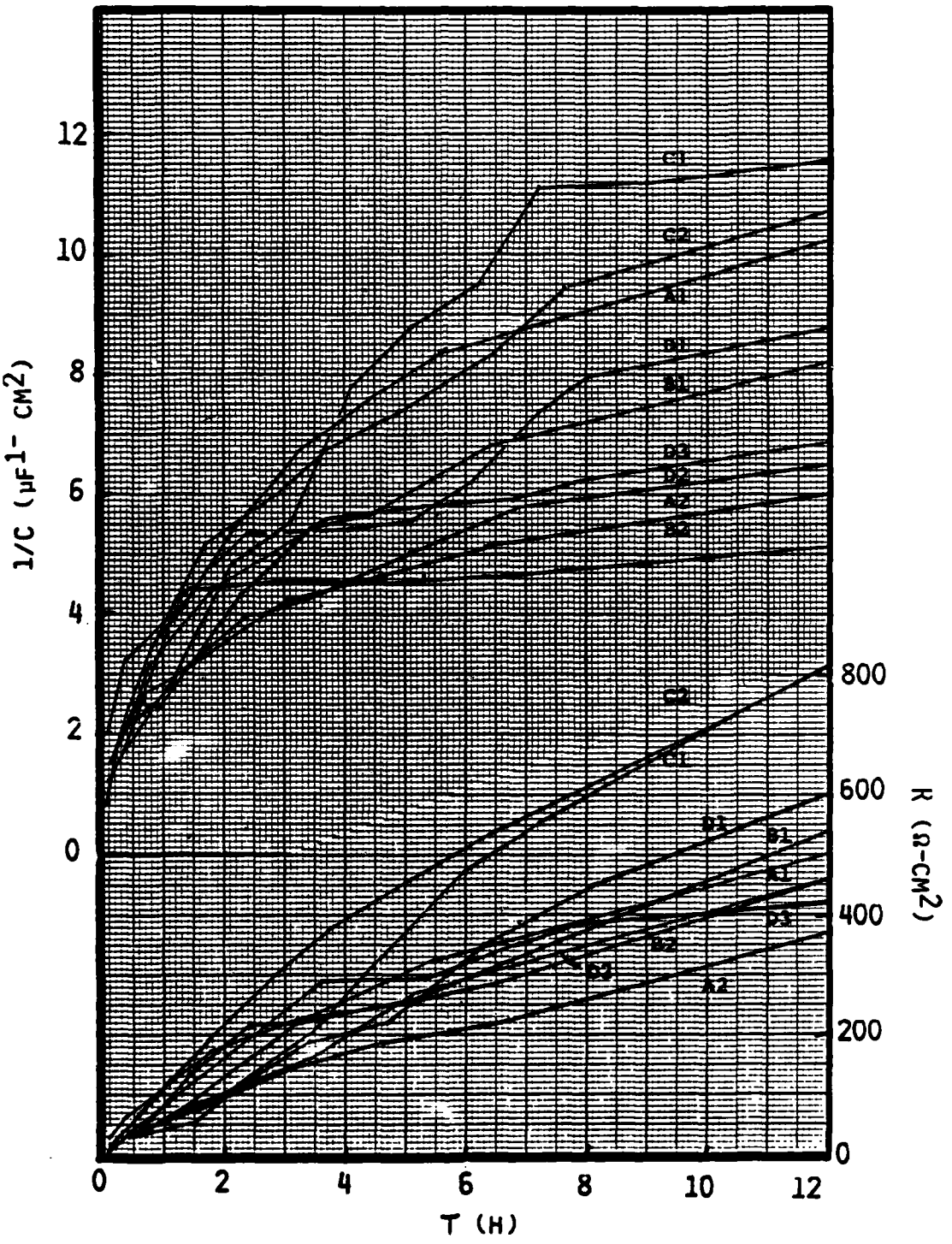

Fig. 12. Inverse capacity and resistances of films grown on fresh Li surfaces in 1.8M $LiAlCl_4/SOCl_2$. Series 7-xxx. Numbers 1,2,3 denotes 1st, 2nd and 3rd cuts of Li in the same electrolyte.

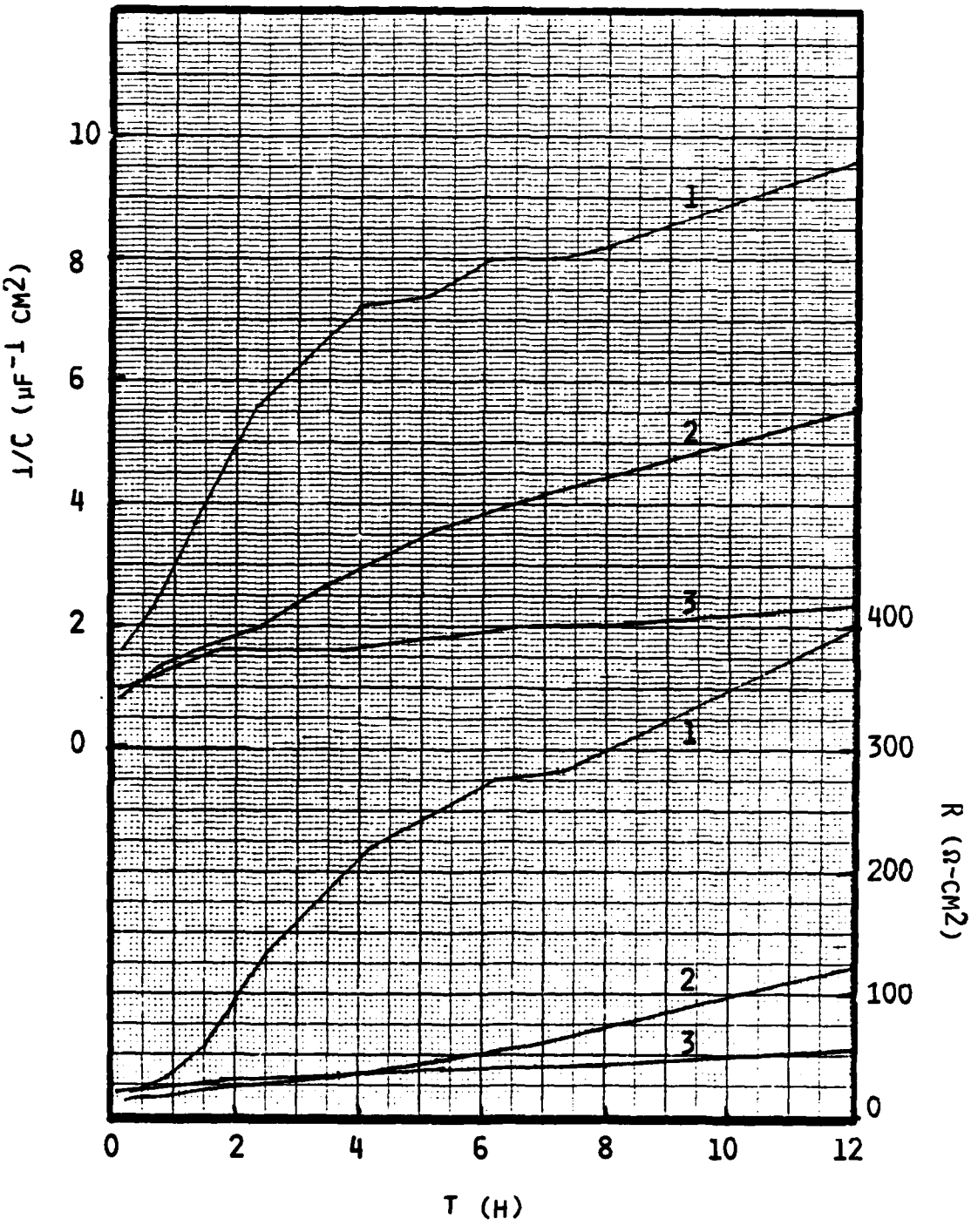

Fig. 13. Inverse capacity and resistance of films grown on fresh Li surfaces in 0.5M $LiAlCl_4/SOCl_2$, experiment 7-05A, 1st, 2nd, and 3rd cut of the Li surface in the same electrolyte.

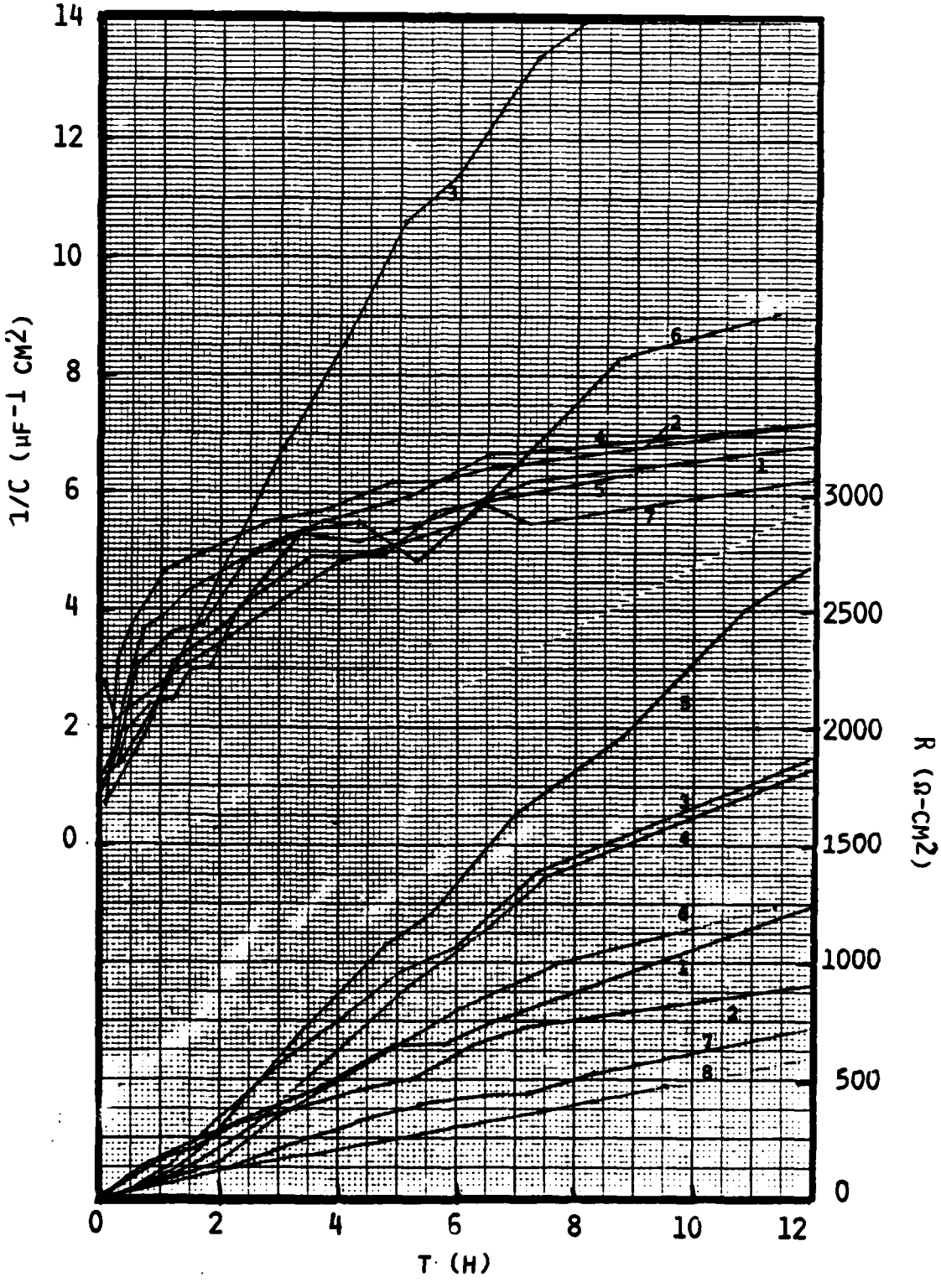

Fig. 14. Inverse capacity and resistance values of films grown on fresh Li surfaces in $LiAlCl_4/SOCl_2$ of varying concentrations. Series 8-xxx. 1, 2 = 1.8M; 3, 4 = 1.0M; 5, 6 = 0.5M; 7, 8 = 0.1M.

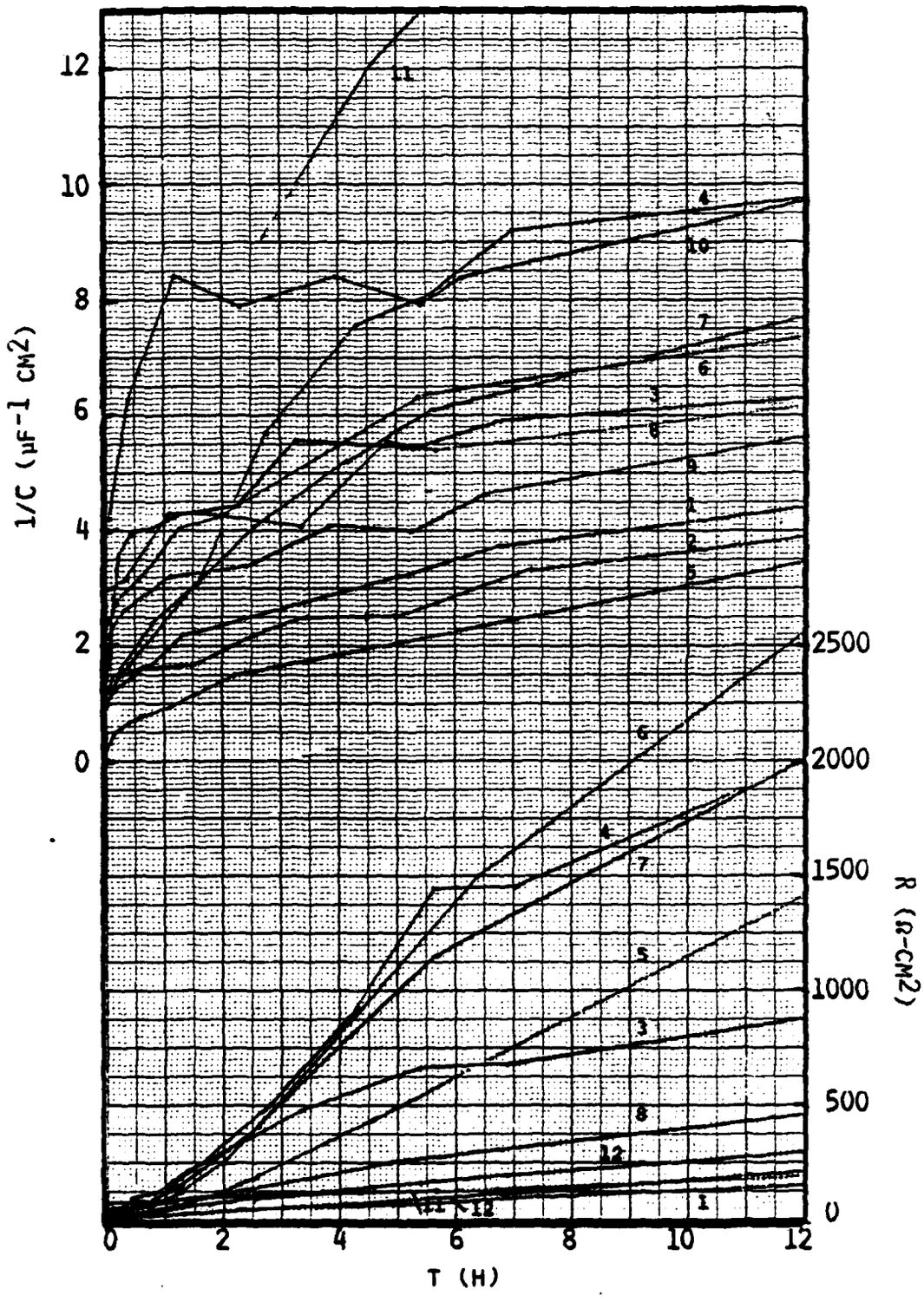

Fig. 15. Inverse capacity and resistance values of films grown on fresh Li surfaces in $LiAlCl_4/SOCl_2$ electrolytes of varying concentrations. Series 9-xxx. 1, 2 = 3.0M; 3 = 2.0M; 4 = 1.0M; 5, 6, 7 = 0.5M; 8 = 0.25M; 9 = 0.1M; 10 = 0.075M; 11, 12 = 0.05M.

TABLE 2

SUMMARY OF MEASURED INVERSE CAPACITY AND RESISTANCE VALUES OF FILMS GROWN ON FRESH Li SURFACES AFTER EXPOSURE FOR 20 HOURS TO VARIOUS $LiAlCl_4/SOCl_2$ ELECTROLYTES

Experiment	Solvent No.	Salt No.	Electrolyte Preparation*	LiCl Equilibration (days)	Electrolyte Age (days)	Electrolyte Concentration (M/L)	Cut No.	$(1/C)_{20}$ (μF^{-1} cm^2)	R_{20} ($\mu\Omega^{-1}$ cm^2)	$d\Omega/dt$ (Ω-cm^2 h^{-1})	ρ_{ap} (Ω-cm x 10^{-6})
1-20D	850		SD	0.06	29	1.8	1	24.6	569	25.4	0.24
30D	850		SD	0.06	34	1.8	1	28.6	566	19.6	0.21
50D	850		SD	0.06	42	1.8	1	37.8	-	25.6	-
90D	850		SD	0.06	35	1.8	1	14.7	466	18.3	0.33
5-10D	321		SD		-	1.8	1	8.99	789	24.2	0.90
30D	321		SD	0.06	94†	1.8	1	4.05	183	6.8	0.58
50D	321		SD	0.06	80†	1.8	1	3.92	219	9.6	0.47
60D	321		SD	0.06	112†	1.8	1	5.22	340	12.7	0.67
6-10D	6291	619	EF	0.2	2	1.8	1	8.74	397	5.4	0.47
20D	6291	619	EF	0.2	11	1.8	1	5.86	404	4.4	0.71
7-18A	7221	619	EF	0.02	14	1.8	1	12.6	732	28.5	0.60
	7221	619	EF	0.02	14	1.8	2	6.60	589	26.8	0.92
18B	7221	619	EF	0.02	14	1.8	1	10.2	855	39.2	0.86
	7221	619	EF	0.02	14	1.8	2	5.86	713	31.0	1.25
18C	7221	619	EF	0.02	19	1.8	1	12.6	1033	35.2	0.84
	7221	619	EF	0.02	19	1.8	2	13.0	1232	51.7	0.98
18D	8251	619	EF	0.02	3	1.8	1	10.4	882	36.1	0.87
	8251	619	EF	0.02	3	1.8	2	7.57	680	27.1	0.93
	8251	619	EF	0.02	3	1.8	3	8.52	880	40.8	1.07
05A	8251	619	EF	0.02	3	0.5	1	12.7	613	25.2	0.50
	8251	619	EF	0.02	3	0.5	2	7.57	224	11.8	0.31
	8251	619	EF	0.02	3	0.5	3	3.08	74	2.7	0.25
05B	8251	619	EF	0.02	8	0.5	1	15.8	1112	32.4	0.73
	8251	619	EF	0.02	8	0.5	2	<18	-	-	-
05C	8251	619	EF	0.02	8	0.5	1	21.6	1601	27.0	0.76
	8251	619	EF	0.02	8	0.5	2	<22.9	-	-	-
05D	971	619	EF	0.04	1	0.5	1	10.6	1448	80	1.41
	971	619	EF	0.04	1	0.5	2	14.5	2529	137	1.80
	971	619	EF	0.04	1	0.5	3	23.8	2655	123	1.15
05E	971	619	EF	0.04	2	0.5	1	8.71	843	45.4	1.00
	971	619	EF	0.04	2	0.5	2	18.7	2176	100	1.20
	971	619	EF	0.04	2	0.5	3	11.3	1882	89.8	1.72
8-18A	9231	619	EF	8	8	1.8	1	7.85	1201	36.6	1.57
18B	9232	619	EF	14	14	1.8	1	8.41	1975	92.5	2.42
10A	1091	830	EF	26	26	1.0	1	23.2	2712	107	1.20
10B	1091	830	EF	28	28	1.0	1	9.53	-	101	-
05A	1091	830	EF	20	20	0.5	1	8.54	4003	156	4.82
05B	1091	830	EF	23	23	0.5	1	-	-	-	-
01A	1091	830	EF	36	36	0.1	1	7.49	1157	50.3	1.59
01B	1091	830	EF	36	36	0.1	1	-	1031	49.9	-
9-30A	11241	1120	EF	24	24	3.0	1	5.35	367	19.1	0.71
30B	11241	1120	EF	34	34	3.0	1	4.76	419	11.0	0.91
	11241	1120	EF	34	34	3.0	2	5.94	419	20.0	0.73
20A	11241	1120	EF	23	23	2.0	1	6.78	1192	37.6	1.81
	11241	1120	EF	23	23	2.0	2	7.64	1352	44.2	1.82
10A	11241	1120	EF	64	64	1.0	1	10.7	2860	104	3.01
	11241	1120	EF	64	64	1.0	2	13.3	3039	84.3	2.35
05A	11241	1120	EF	14	14	0.5	1	9.25	2460	130	2.74
05B	11241	1120	EF	15	15	0.5	1	8.48	3762	195	4.56
05C	11241	1120	EF	44	44	0.5	1	9.68	3075	139	3.27
025A	11241	1120	EF	72	72	0.25	1	7.11	689	29.0	1.00
01A	11241	1120	EF	64	64	0.10	1	7.03	1129	71.0	1.65
0075A	11241	1120	EF	72	72	0.075	1	11.5	1632	111	1.46
005A	11241	1120	EF	34	34	0.050	1	16.0	271	9.9	0.18
005B	11241	1120	EF	44	44	0.050	1	27.5	521	19.9	0.20

*SD = Successive dilution; EF = pre-electrolyzed fused salt.
†Electrolyte stored over Li.

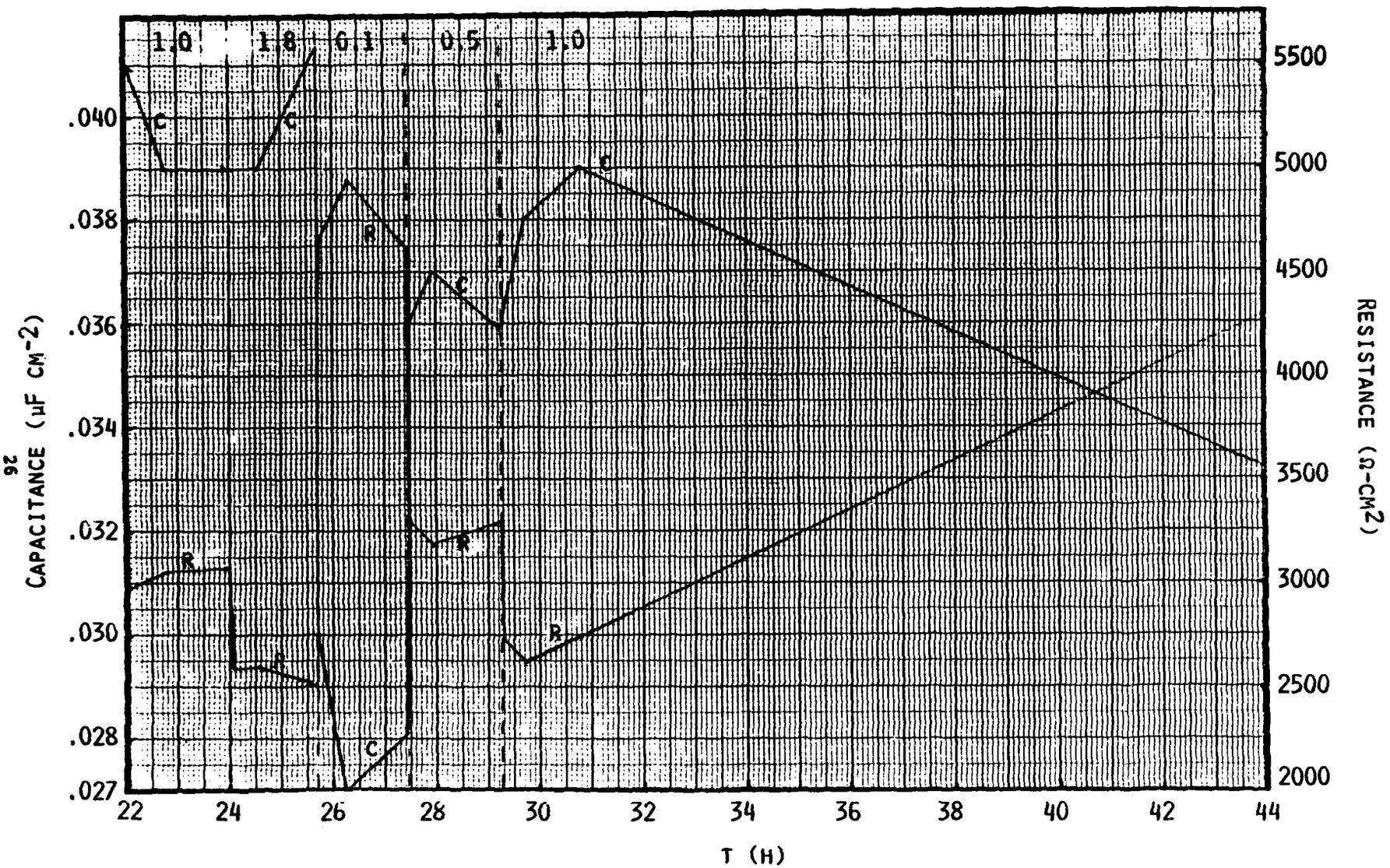

Fig. 16. Resistance and capacity measured in experiment 8-10A upon substitution of the electrolyte. Numbers show $LiAlCl_4$ concentration in mol/ℓ.

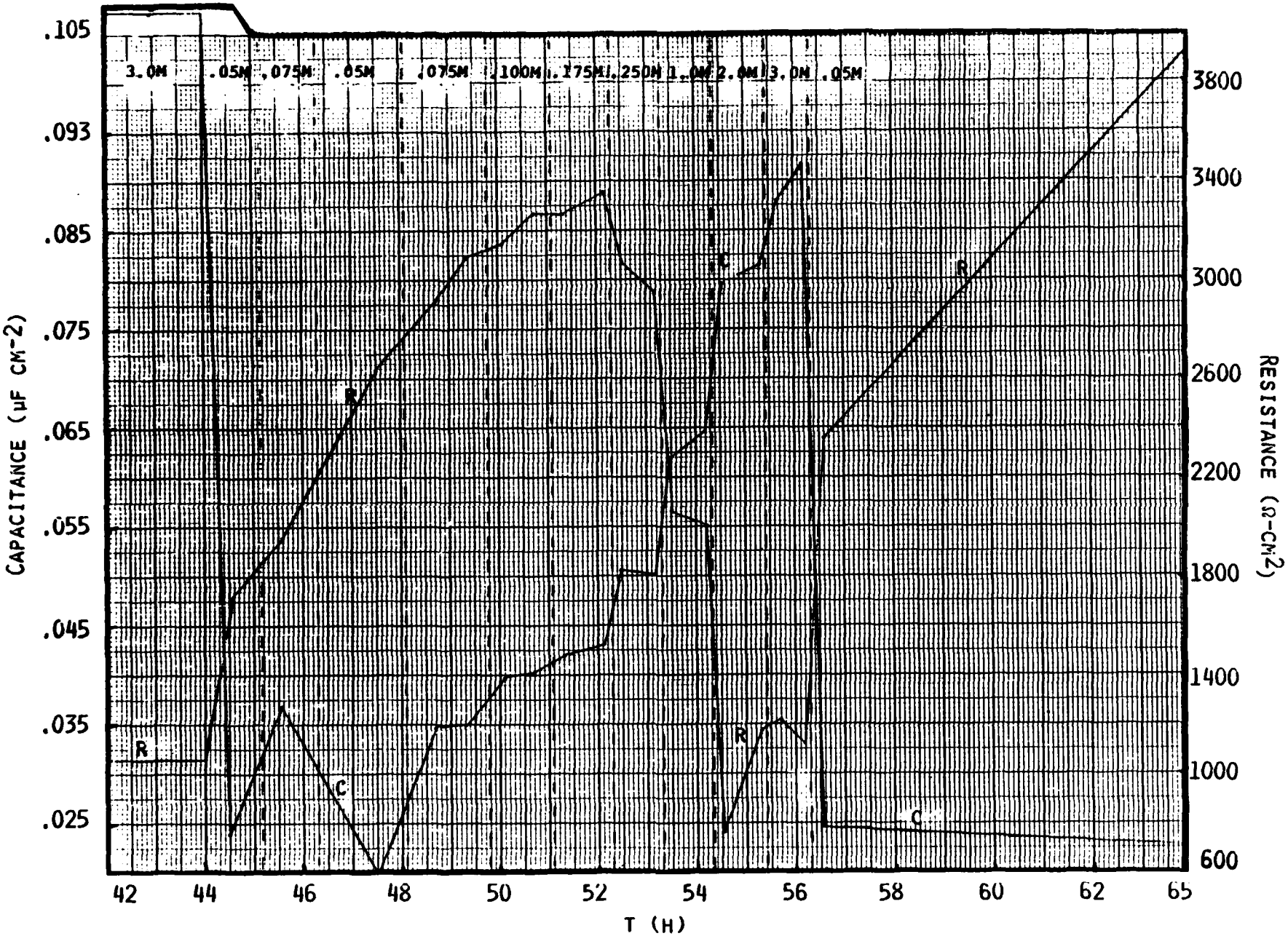

Fig. 17. Resistance and capacity measured in experiment 9-30B upon substitution of the electrolyte. Numbers indicate $LiAlCl_4$ concentration in mol/ℓ.

TABLE 3

CHANGES IN CAPACITANCE AND RESISTANCE OF PREGROWN FILMS IMMERSED IN ELECTROLYTES OF DIFFERENT CONCENTRATIONS

Experiment & Age of Film	Electrolyte Concentration (M)	Capacitance ($\mu F/cm^2$)	$1/C$ (μF^{-1} cm^2)	Resistance (Ω-cm^2)
	3.00	0.107	9.35	1054
	0.05	0.022	45.4	-
	0.075	0.035	28.7	-
9-30A	0.10	0.040	25.0	-
	0.125	0.043	23.5	3353
44 hours	0.250	0.050	20.0	3012
	1.00	0.064	15.8	2036
	2.00	0.081	12.4	971
	3.00	0.090	11.1	1122
	3.00	0.104	9.62	1123
	2.00	0.106	9.43	1094
9-30B	1.00	0.093	10.71	1156
	0.50	0.083	12.1	1520
48 hours	0.25	0.066	15.3	1964
	0.125	0.047	21.3	2532
	0.075	0.038	26.3	2878
	3.00	0.124	8.07	1115
8-18B	1.80	0.108	9.26	2365
	0.10	0.054	18.5	3557
28 hours	0.50	0.080	12.5	3086
	1.00	0.039	25.6	3067
8-10A	1.80	0.041	24.4	2514
	0.10	0.028	36.4	4631
24 hours	0.50	0.036	27.8	3281
	1.00	0.039	25.6	2742
	1.00	0.072	13.9	7886
8-10B	0.50	0.089	11.2	7894
	0.10	0.037	27.0	7779
73 hours	1.80	0.071	14.1	6889
	1.00	0.067	14.9	6748
8-05A	0.50	0.115	8.70	5368
	1.80	0.141	7.09	4420
31 hours	0.10	0.047	21.3	6218
	0.10	0.118	8.48	1322
8-01A	1.80	0.234	4.27	692
	1.00	0.215	4.65	923
25 hours	0.50	0.192	5.21	1178
	0.10	0.108	9.26	1461
	0.075	0.027	37.7	7915
9-075A	0.10	0.041	24.4	7720
	0.50	0.019	12.7	5934
71 hours	2.00	0.093	10.8	4735
	0.075	0.039	25.6	7685

demonstrating that no major changes or damage to the film seems to have occurred as evidenced by nearly identical C and R values after returning to the initial electrolyte concentration following the series of concentration variations.

A closer analysis of these changes shows that a plot of inverse capacity vs. inverse concentration results in a fairly good linear relationship, see Figure 18. This allows us to obtain an extrapolated capacity at infinite electrolyte concentration which would represent the film capacity in a simplified equivalent circuit such as shown in Figure 19. C_E could reflect an electrolyte concentration dependent interface capacity or a double layer capacity in the diffuse layer.

The variation of the measured resistance with electrolyte concentration or probably more relevantly with electrolyte conductivity suggests some film porosity.

If we consider the simplified equivalent circuit of Figure 19, we can divide the measured overall resistance, R_{Exp} into the components R_{F_1} and R_{F_2} of the solid film and R_p of the electrolyte in the film pores as follows:

$$\frac{1}{R_{Exp}} = \frac{1}{R_{F_1} + \frac{R_{F_2} \cdot R_p}{R_{F_2}+R_p}} \qquad (1)$$

If R_{F_1} is small, that is, if the pores penetrate deep into the film the equation simplifies to

$$\frac{1}{R_{Exp}} = \frac{1}{R_{F_2}} + \frac{1}{R_p} \qquad (1a)$$

Assuming further that $1/R_p$ is proportional to the electrolyte conductivity (χ) a plot of $1/R_{Exp}$ vs. χ should yield straight lines. The intercept with the ordinate yields $1/R_F$. Such a plot is shown in Figure 20. Most data follows the linear relationship fairly well. In some cases the $1/R_{Exp}$ values form a concave line which would be in agreement with Eq. (1) if R_{F_1} is not negligible.

If we assume as a first approximation pores which penetrate the main thickness of the film and an electrolyte conductivity within the pores equal to the bulk electrolyte we can estimate a minimum effective cross sectional area of the pores. Values calculated for the various films are summarized in Table 4.

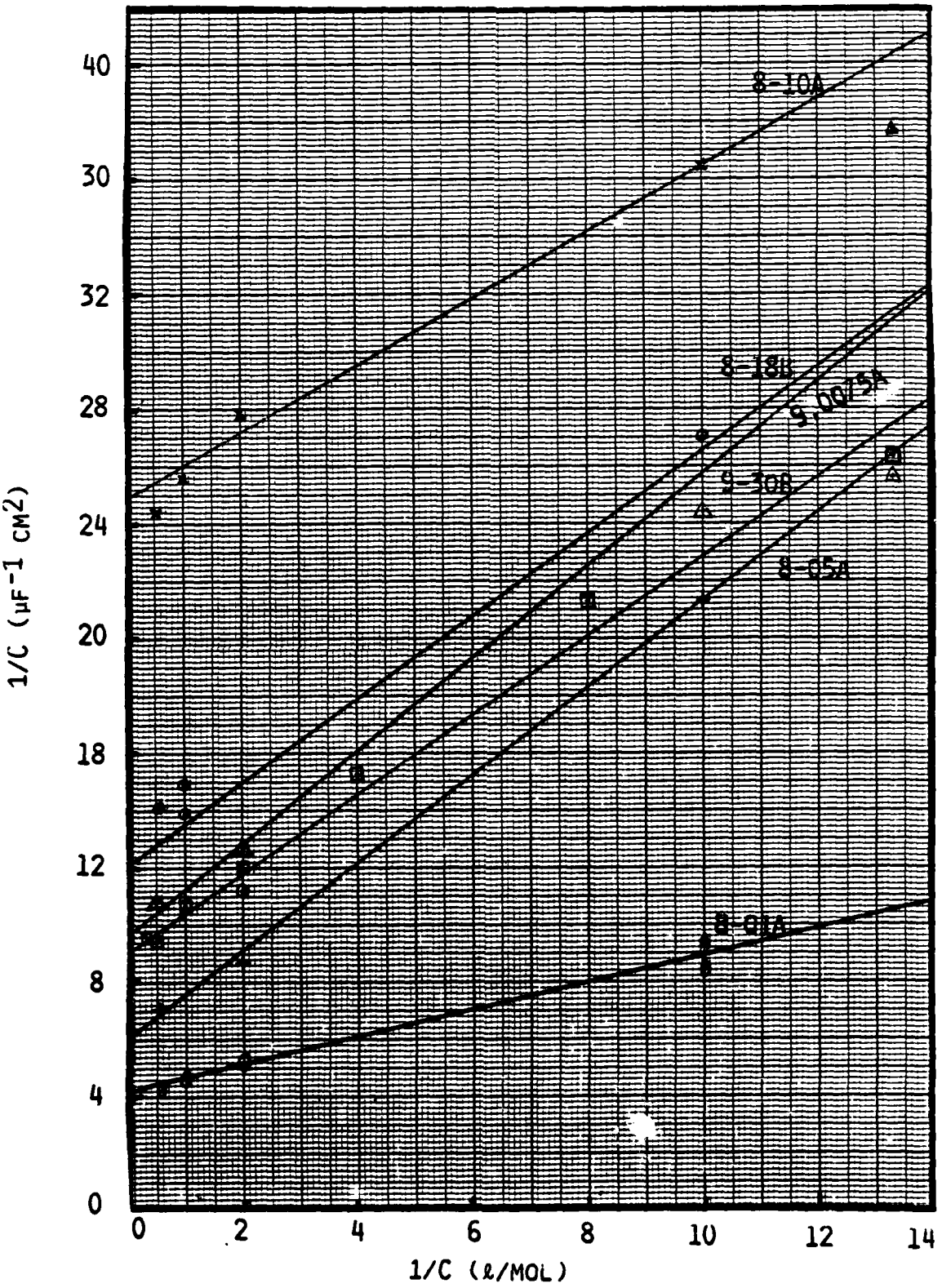

Fig. 18. Inverse capacity vs. inverse concentration. X = 8-10A; O = 8-18B; Δ = 9.0075A; □ = 9-30B; + = 8-05A; 0 = 8-01A. Lines have been derived from a least squares regression.

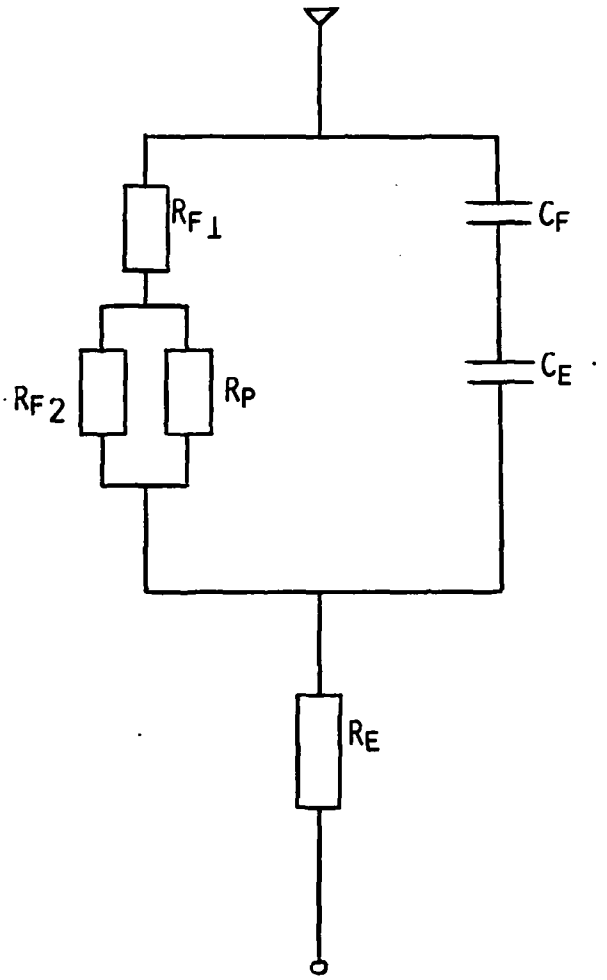

Fig. 19. Simplified equivalent circuit representing film capacitance and resistance.

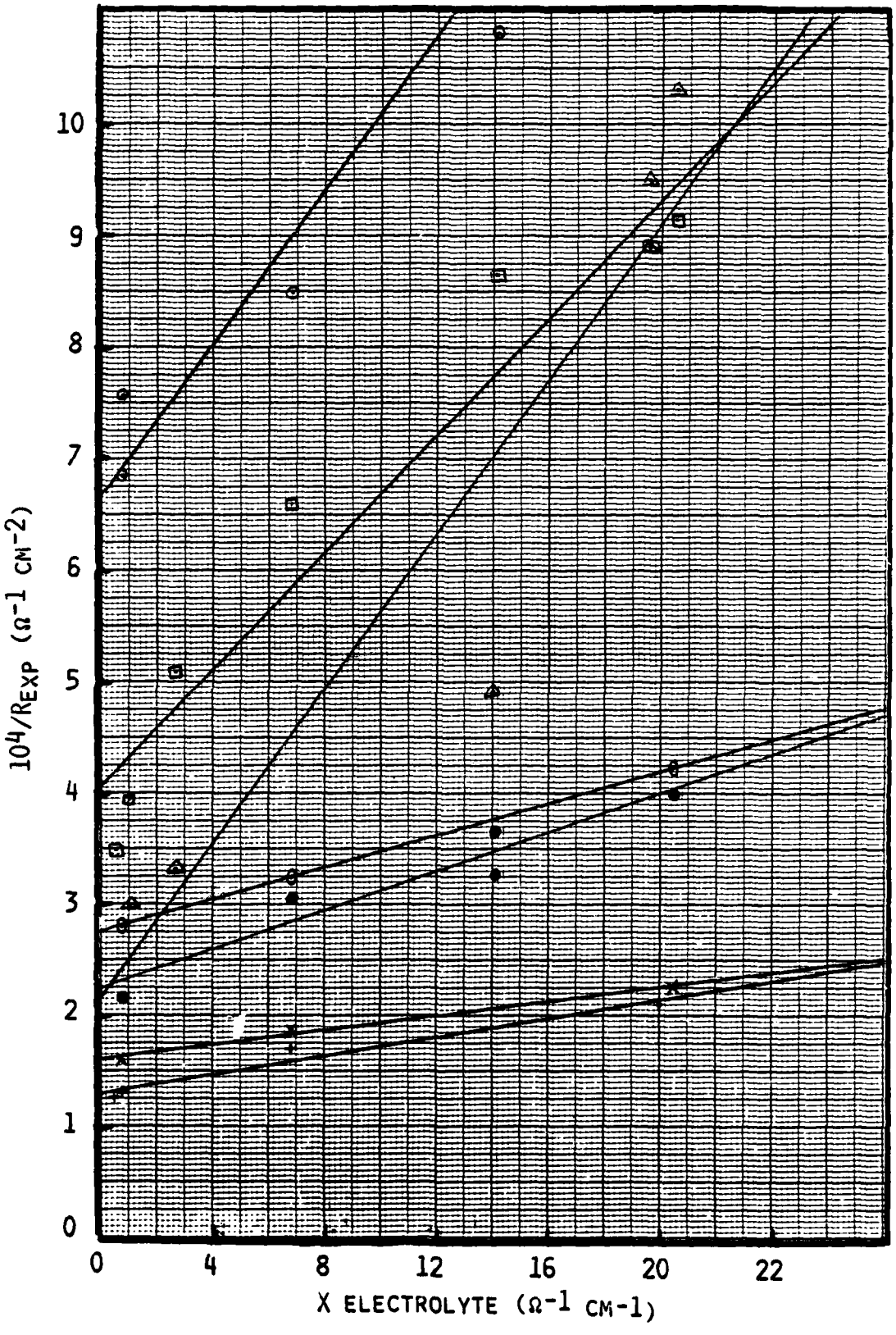

Fig. 20. ($1/R_{exp}$) vs. electrolyte conductivity. Experiments represented are O = 8-01A; Δ = 9-30A; □ = 9-30B; 0 = 8-18B; ● = 8-01A; X = 8-05A; + = 9-0075A.

TABLE 4

ESTIMATE OF MINIMUM Li FILM POROSITY FROM THE DEPENDENCE OF THE OBSERVED FILM RESISTANCE ON ELECTROLYTE CONCENTRATION

Experiment	Lim R^1 C→0 (Ω-cm^2)	R (C=1M) (Ω-cm^2)	Lim $(1/C)^1$ C→∞ (μF^{-1} cm^2)	$d_\infty{}^2$ (cm x 10^{-8})	θ^3 (cm^2/cm^2)	$\rho_o{}^4$ (Ω-cm) x 10^{-8}
8-10A	4476	2484	24.4	2294	3 x 10^{-7}	1.95
8-18B	3631	2366[1]	9.25	870	1 x 10^{-7}	4.17
8-05A	6222	4413	5.97	561	3 x 10^{-8}	11.1
8-01A	1506	725	4.14	389	2 x 10^{-7}	3.87
9-30B	2473	1058	9.05	851	3 x 10^{-7}	2.91
9-075A	7769	4649	9.65	899	6 x 10^{-8}	8.64

[1]Values determined by extrapolation or interpolation of best-fit line.

[2]$d_\infty = (1/C)_\infty \cdot 9.4 \times 10^{-7}$. It is assumed that the thickness of the porous layer is of the same order as the total film thickness and that the limiting inverse capacitance is a good measure of the total film thickness.

[3]If R_{F_1} can be ignored, then

$$\frac{1}{R_{exp}} = \frac{1}{R_{F_2}} + \frac{1}{R_p}$$

$$\frac{1}{R_{exp}} = \frac{1}{R_{F_2}} + \frac{\theta}{\rho d_\infty}$$

and

$$\theta = \rho d_\infty \left[\frac{1}{R_{exp}} - \frac{1}{R_{F_2}}\right]$$

Where ρ and R_{exp} correspond to the 1M values, and $R_{F_2} = \lim_{C\to 0} R$

[4]$\rho_o = R_{F_2}/d_\infty$.

3. Analysis of Voltage Transients

If the film growing on the Li electrode surface can be described by a simple network of a resistor and capacitor in parallel, then the voltage rise as a function of time upon application of a galvanostatic current pulse would be described by

$$V = Ri(1-\exp(-t/RC))$$

where R = resistance, C = capacitance, t = time elapsed since initiation of the current step function. Ri will be the plateau value of the voltage and the relaxation time τ would be the time needed to reach 1-1/e or ~63% of Ri.

Examination of the micropolarization voltage transients revealed that the voltage transients cannot be described by a single exponential relationship as shown above. A good agreement with experimental results can however be achieved by a double exponential curve fit of the following form:

$$\frac{V}{i}(t) = R_1(1-e^{-t/\tau 1}) + R_2(1-e^{-t/\tau 2})$$

$$R_1 + R_2 = R$$

R = measured film resistance at $t \to \infty$.

The double exponential curves fit to the experimental V/i vs. t data are optimized by finding the minimum root mean square deviation of the theoretical curve from the experimental points. The good double exponential fit of the experimental data is illustrated in Figure 21. Calculated τ values are tabulated in Table 5. The data lends support to a dual film model such as, e.g., a compact film which is covered by a porous film. It is tempting to assign $R_1\ \tau_1$ and $R_2\ \tau_2$ to these film components but we believe that this would exceed the significance of this analysis.

4. Film Growth Kinetics

In a first approximation the film on the Li surface may be viewed as a parallel plate capacitor and then its thickness can be derived from the following relationship.

$$d = 8.85 \cdot 10^{-8}\ \varepsilon\ \sigma\ 1/C \qquad (2)$$

where d = film thickness (cm), ε = dielectric constant, σ = roughness factor, C = capacity ($\mu F/cm^2$). Thus the film thickness is directly proportional to the inverse capacity. Plots of inverse capacity vs. time have

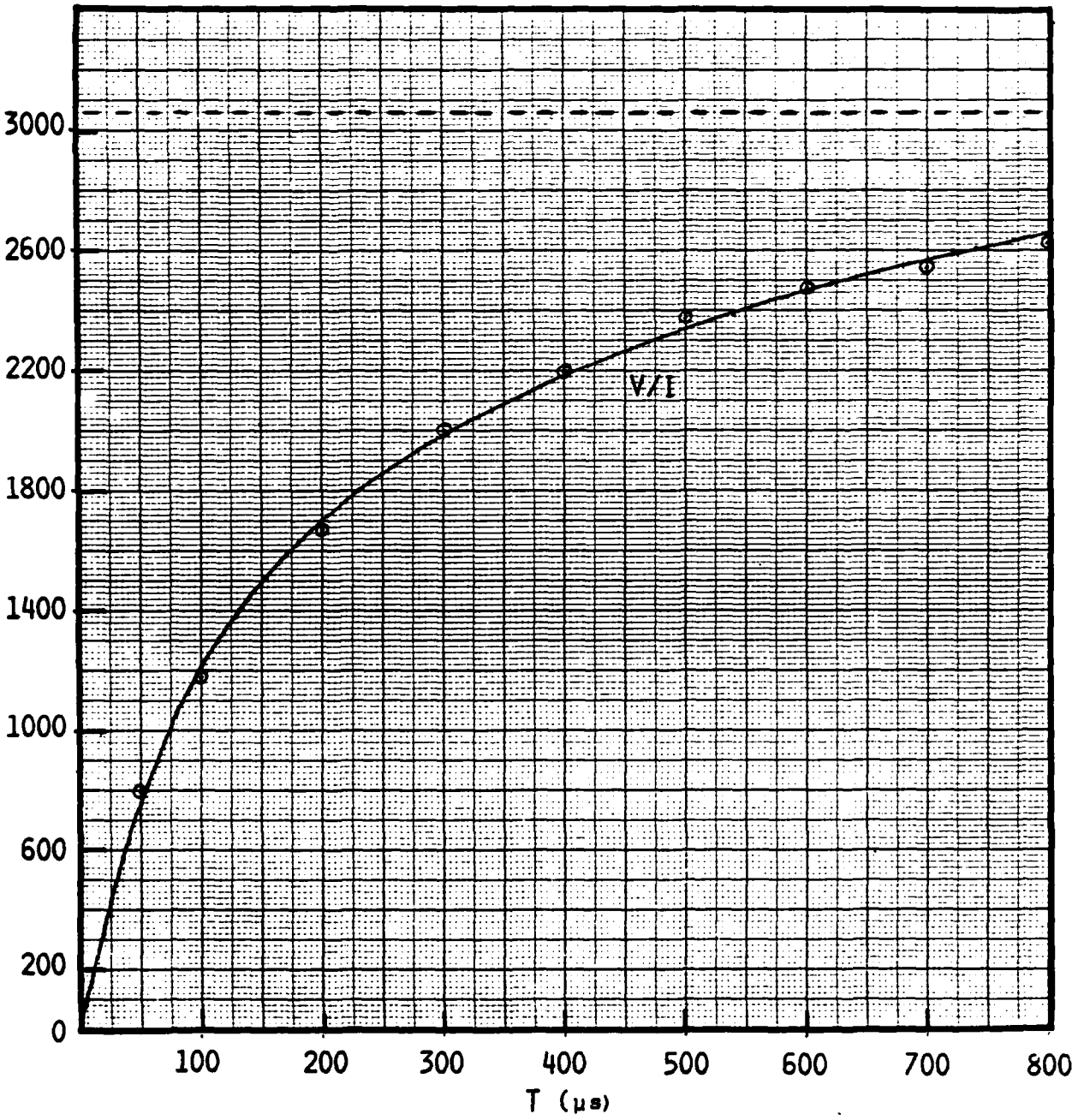

Fig. 21. Normalized voltage-time transient. Theoretical curve (cf. Table 4) is compared to experimental data points from Experiment 8-10A. Dashed line indicates value as $T \to \infty$.

TABLE 5

VOLTAGE-TIME TRANSIENT PARAMETERS ACCORDING TO THE EQUATION

$$\frac{V}{i}(t) = R_1(1-e^{t/\tau_1}) + R_2(1-e^{t/\tau_2})$$

Experiment	Age of Film (h)	R_1 (Ω)	τ_1 (μsec)	R_2 (Ω)	τ_2 (μsec)
8-10A	1.97	142	367	200	81
	5.08	527	420	445	65
	7.32	782	456	616	63
	23.27	1880	517	1175	73
9-30A	6.85	31	206	84	54
8-10B	72.93	6838	1004	1044	101

been summarized in Figures 8 to 15. Often we observed apparently random fluctuations in the capacity-time behavior as shown for example in Figure 22. Corresponding fluctuations were also observed in the resistance measurements suggesting possibly that they are of real significance and may be the result of cracking or restructuring in the surface film.

Examination of the 1/C vs. t plots shows in most cases an initial parabolic region which is then followed by a more asymptotic one. Characteristic examples are shown in Figure 23. In some cases the early film growth is slower than expected from a parabolic relationship possibly suggesting the existance of an induction period.

In a first approximation the overall rate of film thickening, V, of the film can be expressed by a film growth rate V_g and a film dissolution or reaction rate V_c:

$$V = \frac{\partial d}{\partial t} = V_g - V_c \qquad (3)$$

With a film growth rate inversely proportional to the film thickness we obtain

$$V = \frac{k}{d} - V_c \qquad (4)$$

With equations 2 and 3 this results in

$$\frac{\partial\ B \cdot 1/C}{\partial\ t} = \frac{k \cdot C}{B} - V_c \qquad (5)$$

where $B = 8.85 \cdot 10^{-8}\ \varepsilon\ \sigma = 9.4 \cdot 10^{-7}\ \mu F/cm$ (σ=1). Figures 24 and 25 shows plots of $\partial\ 1/C/\partial t$, obtained by graphical differentiation of the 1/C vs. t plots, against C. The data follows fairly well the linear relationship predicted by Equation 4. From the slope we obtain the film growth rate constant k and from the intercept on the abscissa the capacity corresponding to the steady state film thickness. From this we can calculate the dissolution rate

$$V_c = \frac{k}{d_\infty} = \frac{k \cdot C_\infty}{B} \qquad (6)$$

Values for the film growth rate constant k and for V_c are summarized in Table 6.

5. Film Resistivity

The resistivity $\rho_f\ \partial R/\partial d$ of films grown on fresh Li surface was determined from the slope of 1/C vs. R plots.

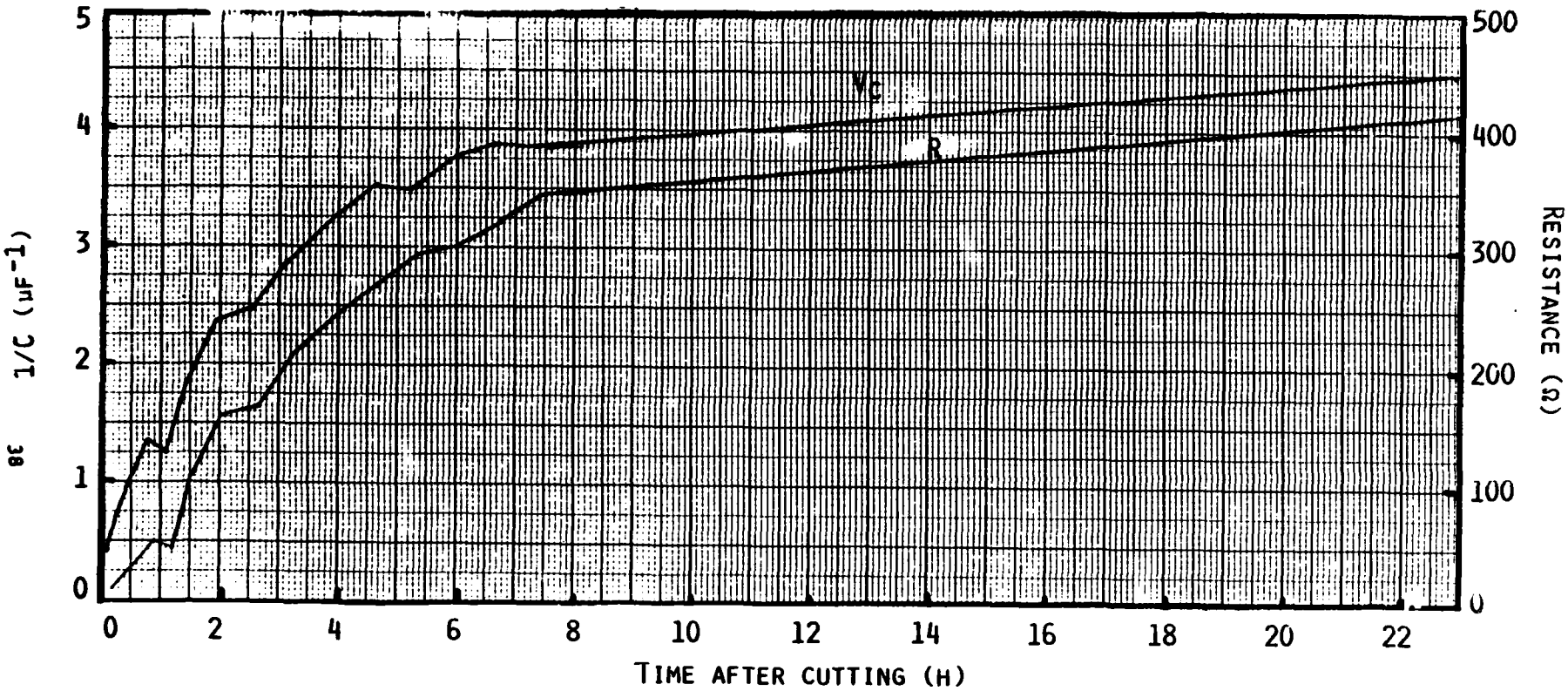

Fig. 22. (1/C) vs. t and R vs. t plots illustrating erratic, parallel changes in R and (1/C). Experiment 6-100.

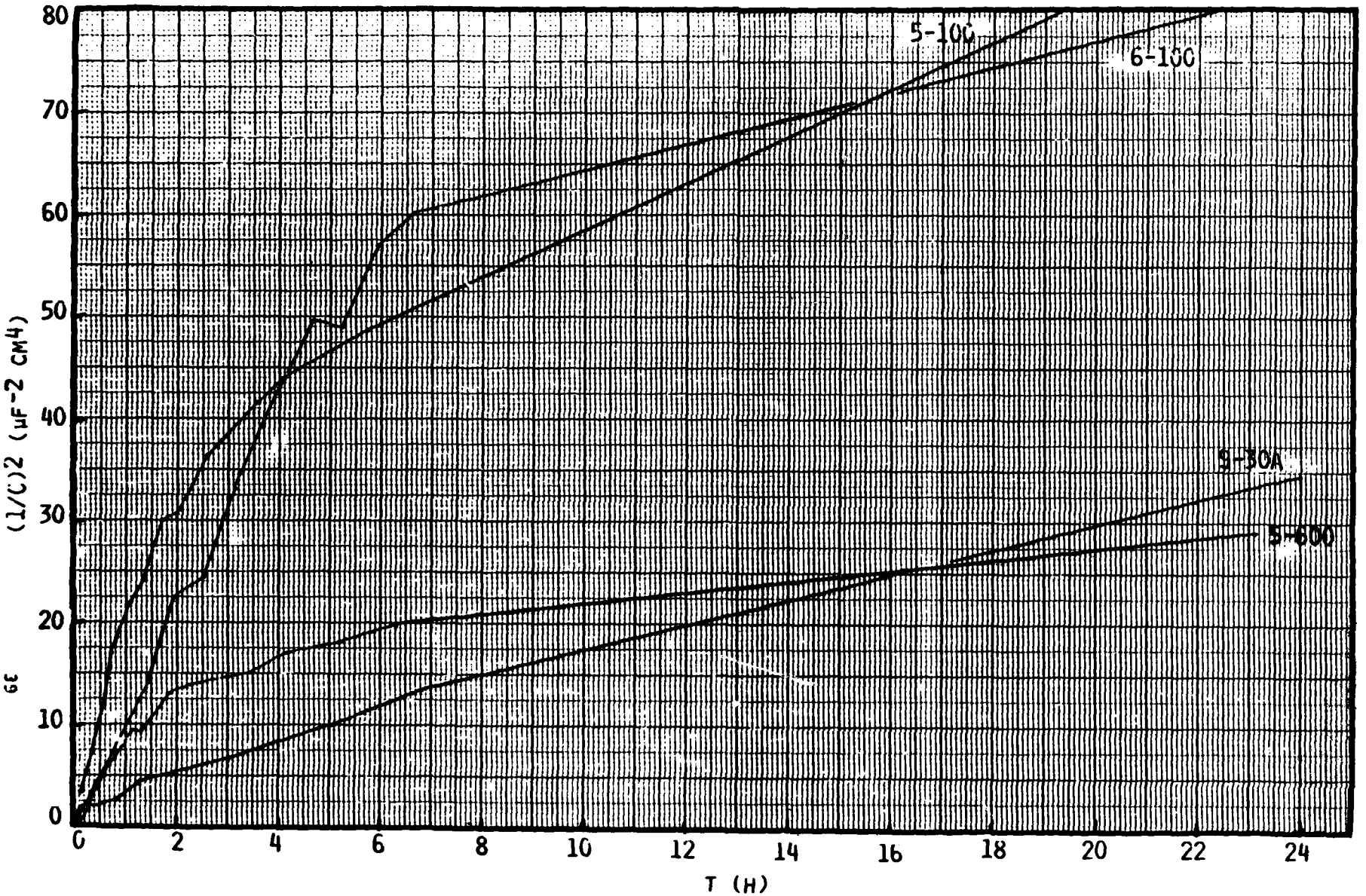

Fig. 23. Inverse square capacitance vs. time plots (parabolic plots).

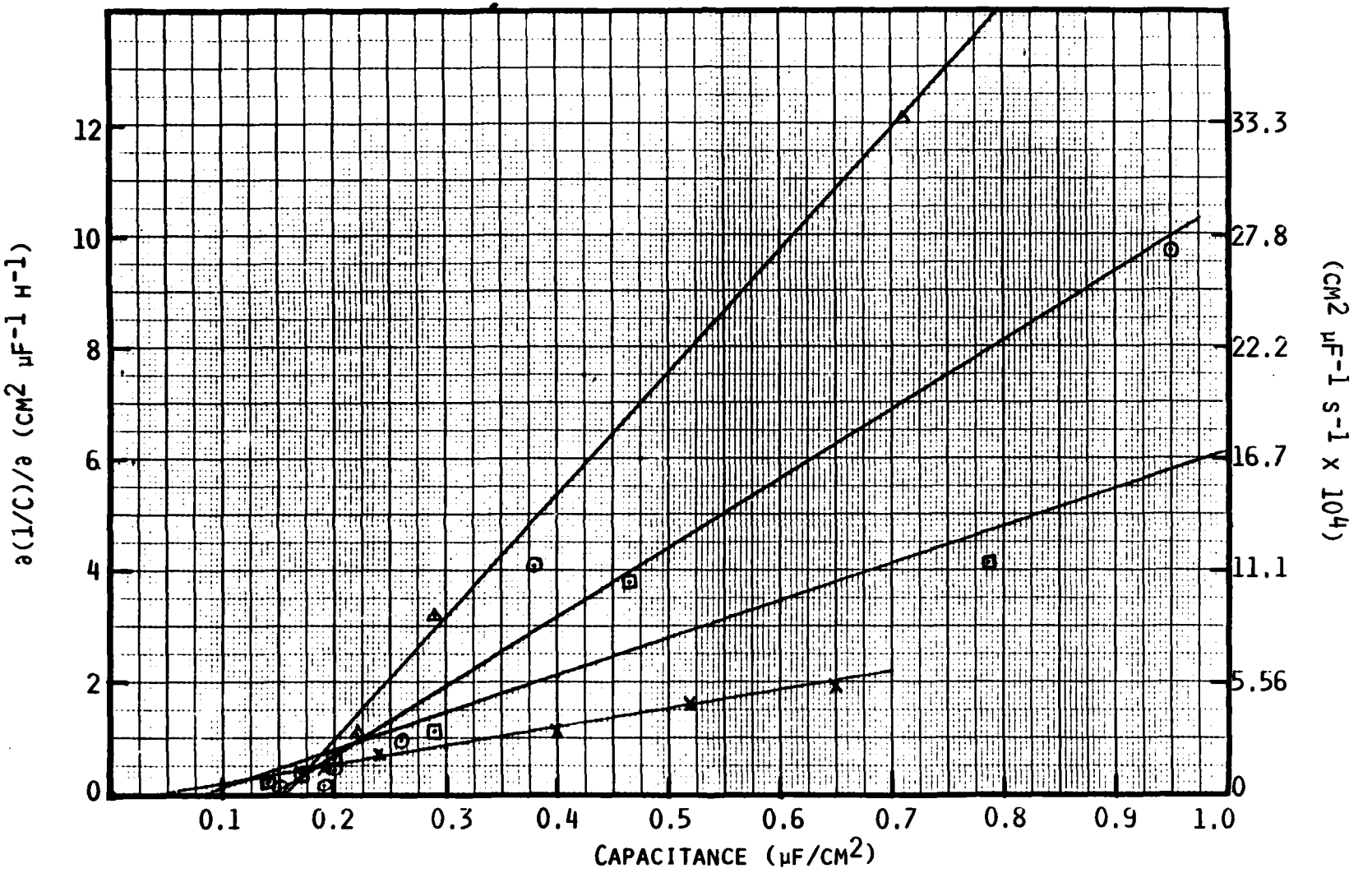

Fig. 24. ∂(1/C)/dt vs. capacitance ⊙ = 8-18A; △ = 8-18B; ⊡ = 8-10B; X = 8-05A.

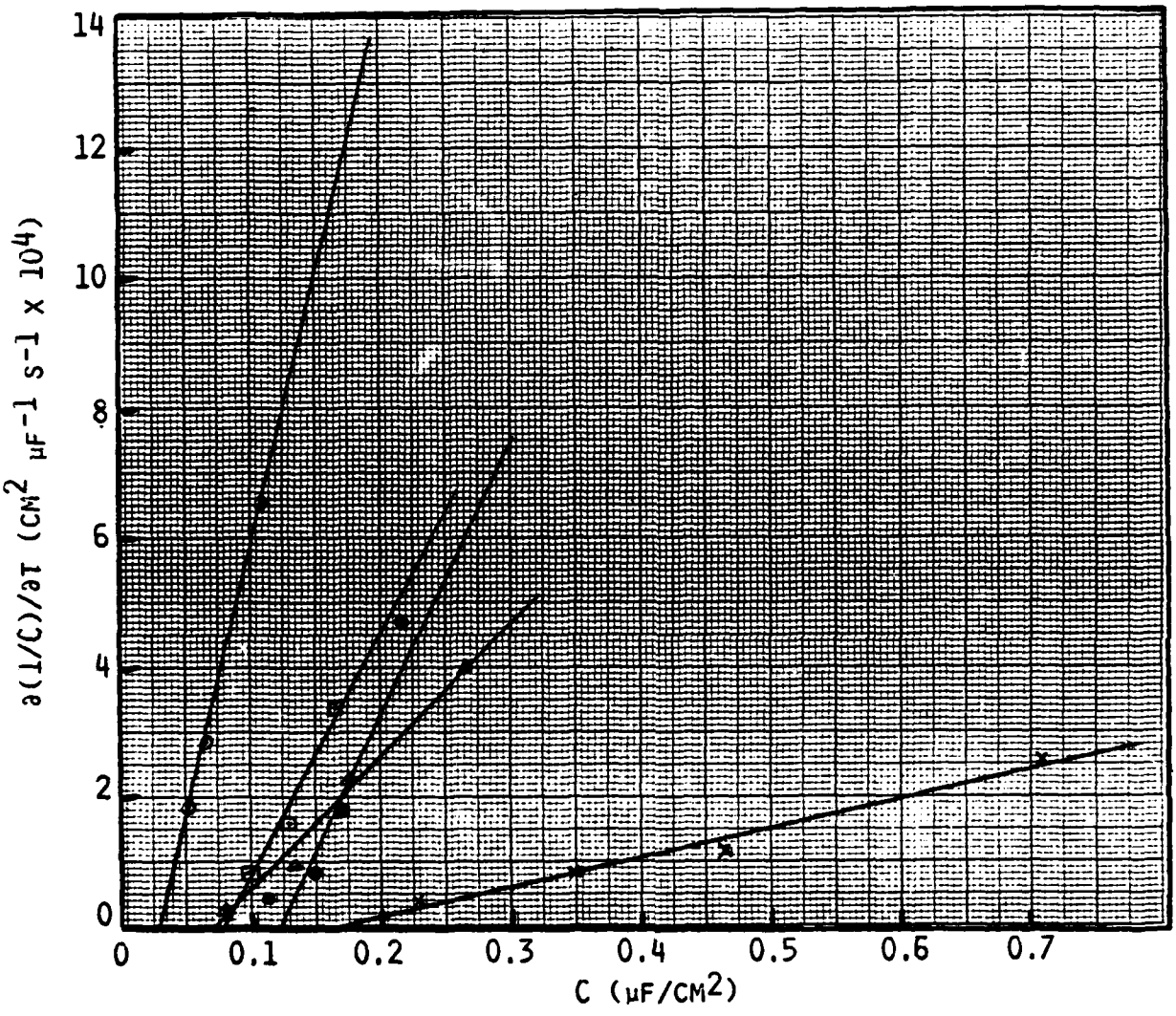

Fig. 25. ∂(1/C)/dt vs. capacitance. 0 = 1-200; ● = 5-100; □ = 7-18A; Δ = 6-100; X = 9-30A.

TABLE 6

RATE CONSTANTS FOR FILM GROWTH AND FILM DISSOLUTION

Experiment	K (cm^2/sec) (x 10^{16})	V_c (cm/sec) (x 10^{10})	d_∞ (Å)	Symbol (Fig. 25)
1-200	75	2.5	3000	o
5-100	37	4.9	762	●
5-600	30	7.9	376	
6-100	18	1.4	1271	Δ
7-18A1	33	2.7	1199	□
2	20	4.2	482	
7-18D1	18	1.7	1105	
2	11	1.3	793	
3	28	5.0	596	
7-05A1	25	2.1	1175	
2	3.1	1.2	264	
3	1.9	0.68	281	
8-18A	30	4.8	635	
8-18B	53	8.8	607	
8-10B	17	1.6	1040	
8-05A	8.3	0.49	1695	
9-30A1	4.1	0.75	545	x
2	6.3	1.5	417	
9-20A1	33	5.9	570	
9-10A1	38	3.4	1106	
2	28	1.5	1880	
9-05A	2.1	0.68	307	
9-05B	16	1.9	854	
9-05C	19	1.9	990	
9-01A	16	3.2	509	

$$\rho_f = \frac{\partial R}{\partial d} = \frac{1}{9.4 \cdot 10^{-7}} \frac{\partial R}{\partial\ 1/C} \quad (\Omega\ \text{cm})$$

Typical data are shown in Figures 26 to 28. We observe clearly two regions and a more or less sharp transition between them. The transition occurs generally between one half and one hour. Resistivities calculated from the early and later slopes are listed in Table 7. The ratio of the maximum to the minimum resistivities is generally between three and twelve. Average values for the early and later resistivities were $2.5 \cdot 10^7$ and 3.10^8 Ωcm respectively.

We evaluated film resistivities also from resistance and capacity measurements which were adjusted by extrapolation for electrolyte contributions as discussed earlier. Such values are summarized in Table 8. The results are very comparable to those obtained from differential changes in R and C.

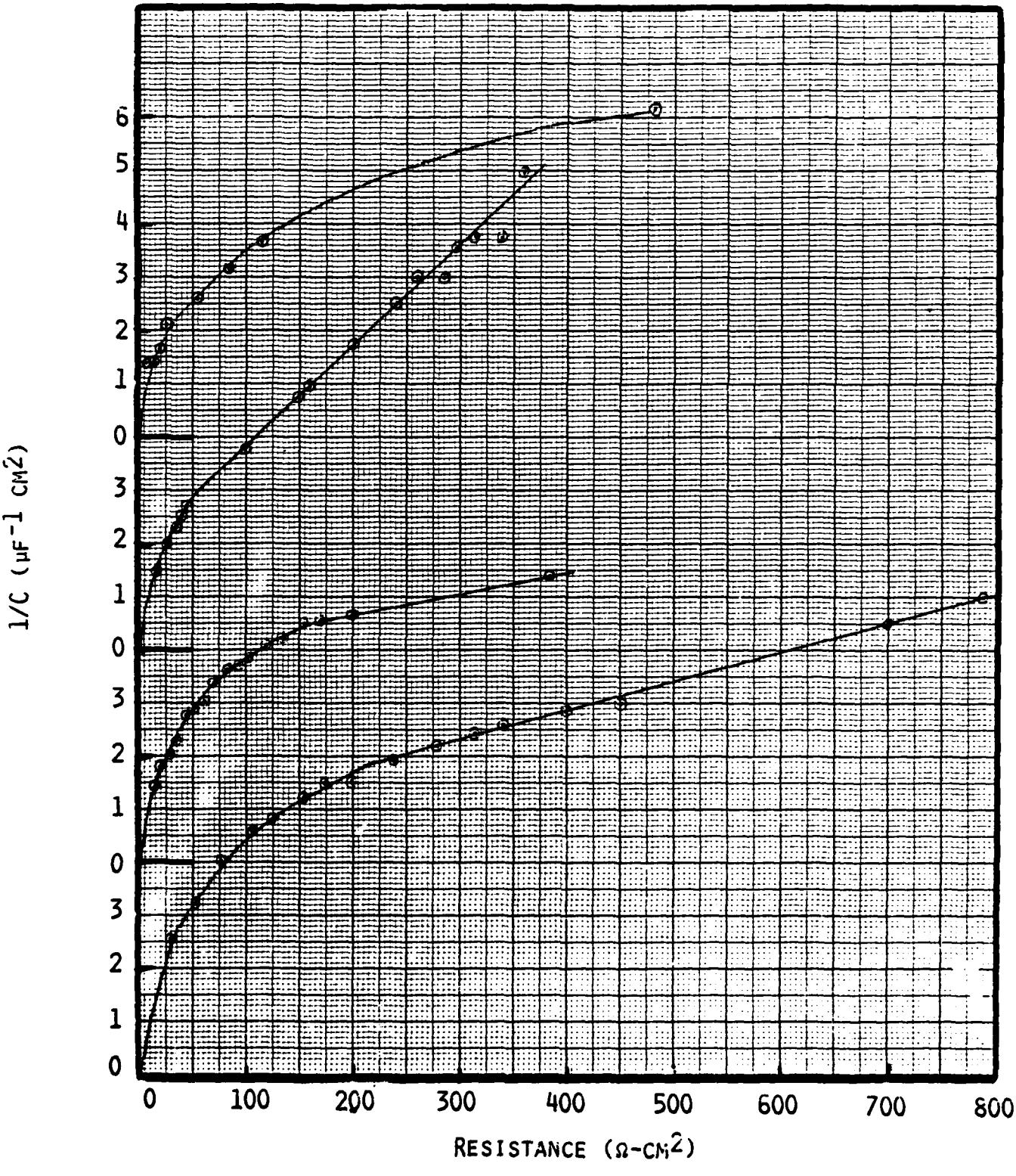

Fig. 26. Inverse capacity vs. resistance. Four curves from bottom to top represent experiments 5-100, 5-600, 6-100, and 9-30A.

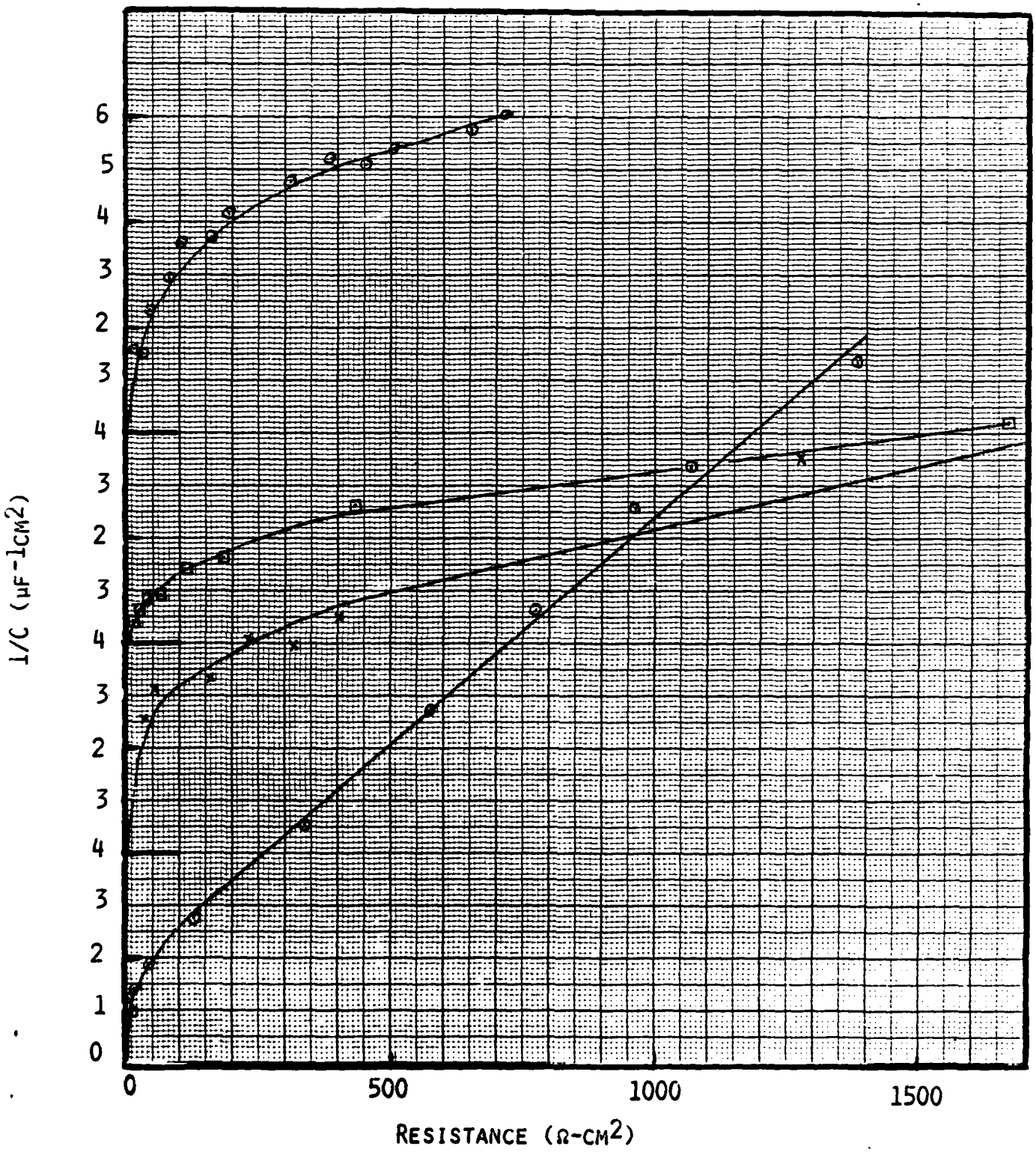

Fig. 27. Inverse capacity vs. resistance. Four curves from bottom to top represent experiments 8-10A, 9-01A, 9-05A, and 8-18A.

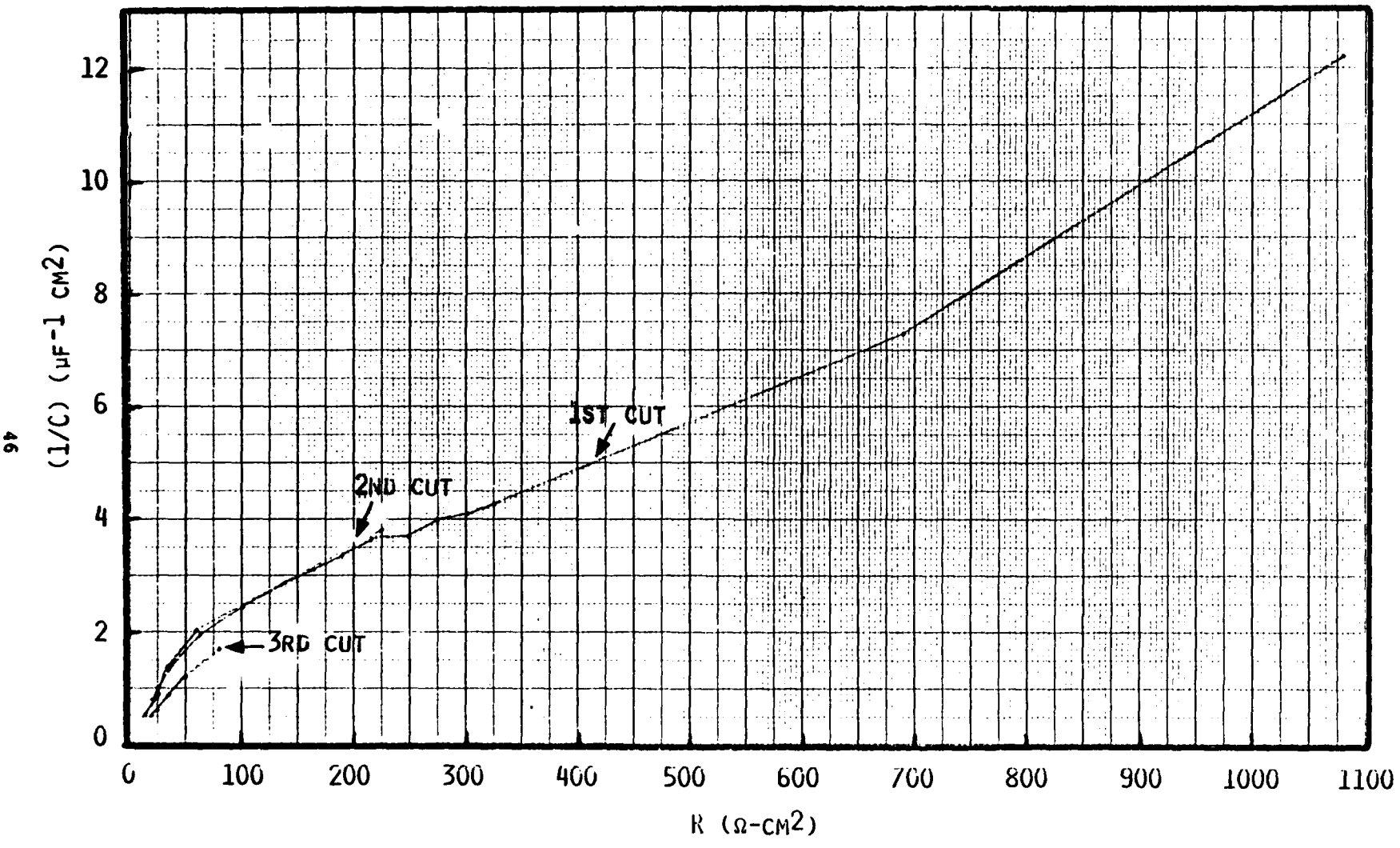

Fig. 28. Inverse capacity vs. resistance for three cuts of experiment, 7-05A.

TABLE 7

SPECIFIC RESISTIVITIES OF FILMS GROWN ON FRESH Li SURFACES

Experiment	Minimum ρ_f (Ω-cm) t < 1 hr	Maximum ρ_f (Ω-cm) t > ~10 h
1-200	5.9×10^6	3.9×10^7
5-100	3.2×10^7	1.9×10^8
5-600	3.27×10^7	5.0×10^8
6-100	1.7×10^7	6.4×10^7
7-18A 1	2.0×10^7	1.1×10^8
2	2.2×10^7	1.04×10^8
7-05A 1	1.3×10^7	7.6×10^7
2	1.0×10^7	5.4×10^7
3	0.9×10^7	3.6×10^7
8-18A	2.7×10^7	3.1×10^8
8-10A	-	1.4×10^8
8-10B	3.3×10^7	6.7×10^8
8-05A	7.1×10^7	1.0×10^9
9-30A 1	1.4×10^7	1.7×10^8
2	1.5×10^7	5.5×10^7
9-30B 1	2.4×10^7	1.0×10^8
2	1.9×10^7	2.5×10^8
9-20A 1	2.7×10^7	3.7×10^8
9-05B	2.5×10^7	1.2×10^9
9-05C	2.5×10^7	5.6×10^8
9-025A 1	2.1×10^7	2.7×10^8
2	3.1×10^7	2.6×10^8
9-01A	1.4×10^7	1.02×10^9
9-005B	5.3×10^6	1.7×10^8

TABLE 8

SPECIFIC RESISTIVITIES OF FILMS GROWN ON FRESH Li SURFACES

Experiment	Film Growth Time (h)	$1/C$, μF^{-1}		R, Ω		ρ_f, $\Omega cm \times 10^{-8}$
		exp	corr(1)	exp	corr(2)	
8-10A	24	25.8	24.8	3500	4444	1.9
8-18B	73	14.0	12.0	2500	3636	3.2
8-05A	31	8.7	6.0	5405	6490	11.5
8-01A	25	9.0	4.2	1460	1492	3.8
9-30B	48	9.5	9.0	1123	2500	3.0
9-0075	71	37.8	9.7	7690	7690	8.4

(1) Extrapolated for electrolyte conc $\rightarrow \infty$.

(2) Extrapolated for electrolyte conductivity $\rightarrow 0$.

IV. DISCUSSION AND CONCLUSIONS

The results of our measurements can best be explained by a three zone film model as shown schematically in Figure 29. Immediately after exposure of a fresh Li surface to the electrolyte a protective film probably of LiCl starts to form on the surface. This film consists of a large number of small crystallites which during their rapid growth give rise to irregular grain boundaries probably with many dislocations and electrolyte inclusions. This film region reached thicknesses between 200 Å and 400 Å in our experiments and its growth is essentially completed in less than an hour. On top of this film a more ordered and more compact layer (Region II) forms. Here the greatly reduced rate of LiCl generation with the dissolution and recrystallization of the less stable small and disordered crystals act together to create well ordered larger crystals with a much reduced yet not completely negligible "porosity" along the grain boundaries. Finally a porous coarse crystalline macroscopic film (Region III) develops. The latter can reach considerable thickness and is clearly observed by microscopy (1,2). This film does not contribute to the transient voltages measured in our present investigation and thus our results cannot be used to draw conclusions about its specific characteristics.

In the following we discuss in more detail the reasons for this film model, its implications and how it agrees or disagrees with other published information.

1. Structure of the Surface Film

Our concept of some film "porosity" is based on the dependence of the measured resistance of a pregrown film on the electrolyte concentration. The "porosity" is very small ($<10^{-7}$ cm^2 pore cross sections per cm^2 film) and can be visualized as occasional small channels along the grain boundaries of individual LiCl crystallites. A similar dependence of the apparent film resistivity on the electrolyte was also observed by Peled et al. (4) who attribute it to an as yet not understood mechanism by which the higher electrolyte solution creates more lattice defects in the film and thus makes it more conductive. Our specific film resistivities from differential thickness and resistance measurements (Table 6) do not support such differences in film properties. For example the specific resistivities of films grown in 3M $LiAlCl_4$ solutions were $1.4 \cdot 10^8$ Ωcm compared with $1.7 \cdot 10^8$ Ωcm for a film grown in a 0.05M $LiAlCl_4$ solution.

A variation of the capacity measured on pregrown films in electrolytes of different concentration was also observed by Peled al al. (4) and Moshtev et al. (6). Speculative explanations involved an effect of

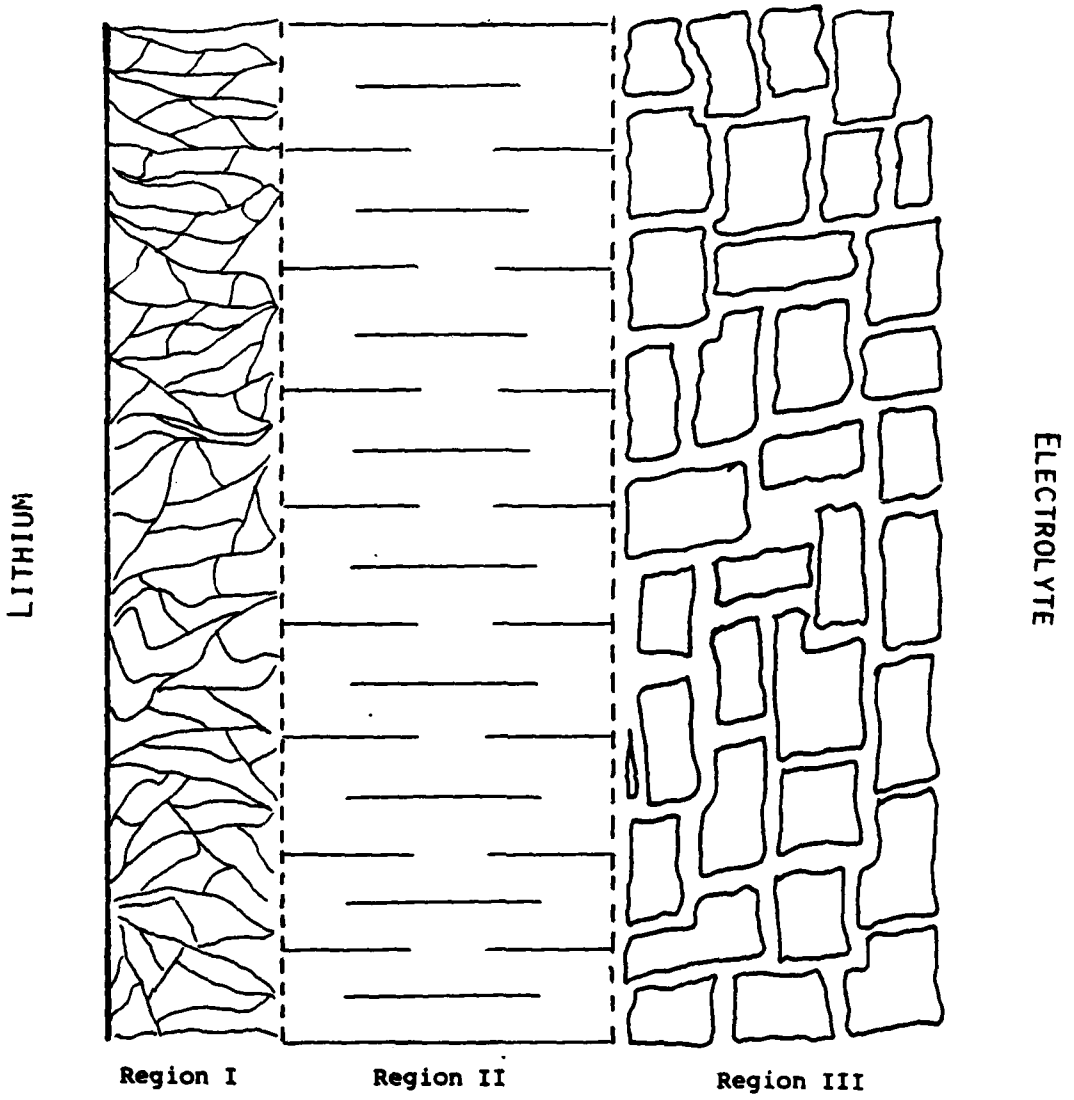

Fig. 29. Schematic illustration of the proposed three region model of the film formed on a fresh Li surface upon exposure to $LiAlCl_4$-$SOCl_2$ electrolytes. Region I - fine crystalline LiCl with microinclusions of electrolyte along grain boundaries. Region II - more compact, well ordered LiCl layer. Region III - porous, coarsely crystalline non-passivating layer.

the electroltye concentration on the dielectric constant of the film and a contribution of the diffuse double layer in the electrolyte. If one accepts the concept of some film porosity an equally plausible explanation would be the increased accessibility of film internal surface area at higher electrolyte conductivities.

Plots of 1/C, which is a measure of film thickness, against film resistance clearly show two regions. Apparent film resistivities derived from this data suggest approximately 2.10^7 Ωcm for the early film (Type I) and approximately a magnitude larger $\sim 2.10^8$ Ωcm for the later film (Type II). This resistivity is very close to the $2.7 \cdot 10^8$ Ωcm expected for undoped LiCl at room temperature (10). We believe that this difference results from an increased disorder or "porosity" along the grain boundaries of the early rapidly growing film rather than from a different conductivity of the LiCl crystals themselves. Such an interpretation is supported by the close correspondence of film resistivities calculated from corrected (film capacity as electrolyte conductivity $\rightarrow \infty$ and film resistance at electrolyte conductivity $\rightarrow 0$) capacity and resistance values (Table 7) with those of film II derived from differential measurements. The decreasing sensitivity of film resistance to changes in electrolyte concentration as the film grows thicker which was observed by Peled et al. (4) is also consistent with our model. Further support for a dual character film can be derived from the analysis of the voltage transients which indicate more than one transition time. A homogeneous film which merely varies in thickness would result in a single transition time τ which would be described by the product of R and C.

Two regions of different shape in 1/C vs. R were also observed by Moshtev et al. (6). The initial higher slope was interpreted as reflecting the progressive displacement of the original oxide film on the Li with LiCl. The slope change was associated with reaching full surface coverage of LiCl. It occurred after approximately 20 min. Such an explanation cannot hold in our experiments where a fresh Li surface is created within the electrolyte solution.

2. Film Growth Kinetics

Film growth mechanisms by galvanic corrosion governed by an electronic current in the film or by diffusion of holes through the solid electrolyte layer as the rate determining step were proposed by Peled (3). Both mechanisms lead to parabolic laws of growth. Our experimental results follow a parabolic relationship during the initial phase but then deviate more and more. This data can be described well by a mechanism proposed by Moshtev et al. (6) involving a constant dissolution rate of the film. Thus the electrochemically measured film is expected to eventually reach a constant value. Within the times of our experiments this was never fully achieved and in this respect our results resemble much more those of Peled

(4) while Moshtev reports fairly thin films which have reached steady state values after only 24 hrs. The dissolving LiCl will reprecipitate probably in a porous coarse crystalline form which is not detected by the capacity measurements but which is observed by microscopy (2,4). This agrees also with the long term linear growth of the macroscopic film as found by Dey (2).

Film growth rate constants and dissolution rates as well as extrapolated final passivating film thicknesses showed considerable variability in our experiments. From the data gathered to date, no clear correlation between these parameters and the growth conditions could be derived. There may be a slight maximum in growth rate at electrolyte concentrations between 1 and 2M $LiAlCl_4$. No convincing correlation between electrolyte concentration and film thickness was observed which agrees with other electrochemical studies (4). We found no correlation between film growth rate, film conductivity and electrolyte equilibration times as suggested by Moshtev et al. (6). An interesting and possibly significant observation is the effect which exposure of electrolyte to Li has on the film growth behavior. Electrolytes which were pretreated with Li (e.g., Series 5-600) resulted in thin passivating films. Analysis showed little change in the growth rate constant but an increased film dissolution rate. In recent experiments similar observations were made even though the results were less consistent.

In efforts to correlate concentrations of impurities and reaction products in the electrolytes with film growth parameters, we performed solution analyses before and after the experiments and made intentional additions of H_2O and SO_2 to the electrolyte. To date the results remained inconclusive probably because film growth is affected at levels which are below normal analytical detection limits.

With our film model and the measured growth kinetics we can develop the following simplified scenario for the growth of a characteristic surface film on fresh Li:

	Film Thickness, Region		
Time	I	II	III
~ 1 h	~300 Å	~ 30 Å	~ 50 Å
~ 8 h	~300 Å	~170 Å	~ 400 Å
~20 h	~300 Å	~350 Å	~1000 Å

Region III films are not included in transient measurements near open circuit conditions. Region I films may have a modified structure along the Li surface. The initial part of this film (~50 Å) forms very rapidly

before our measurements started. After 20 hrs film II grows only slowly while most of the growth is in region III. The latter is based on the assumption that most of the dissolved LiCl will reprecipitate within this region. On electrodes which are already covered by a preexisting surface film (e.g., oxide) the film may inhibit the initial rapid reaction thus leading to earlier Region II film formation resulting in a thinner Type I region.

V. REFERENCES

1. A. N. Dey, Thin Solid Films, 43 (1977) 131.

2. A. N. Dey, Electrochimica Acta, 21 (1976) 377.

3. E. Peled, J. Electrochem. Soc., 126 (1979) 2047.

4. E. Peled and H. Yamin, Israel Journal of Chemistry, 18 (1979) 131.

5. R. G. Keil, W. E. Moddeman, T. N. Wittberg, J. R. Hoenigman, P. S. Zaidain and J. A. Peters, U.S. Government Report AFWAL-TR-80-2094, October 1980.

6. R. V. Moshtev, Y. Geronov and B. Puvesheva, J. Electrochem. Soc., 128 (1981) 1851.

7. C. R. Schlaikjer, Progress Batteries and Solar Cells, Vol. 4 (1982) 40.

8. A. M. Hermann, Lithium Batteries, J. Electrochem. Soc., Pennington, NJ, Proc. 1981-4.

9. A. Meitav and E. Peled, J. Electroanal. Chem. 134 (1982) 49.

10. Y. Haven, Rec. Trav. Chim. Pays Bas, 69 (1950) 1476.

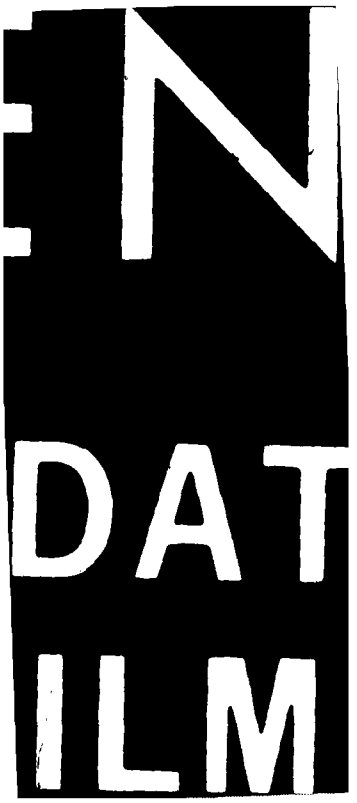
N
DAT
ILM